



Center for Advanced  
Communications

Villanova University

---

**FINAL TECHNICAL REPORT**

**Processing for Interference Suppression  
in GPS Receivers**

*May 2004-September 2005*

Submitted to

**Office of Naval Research**

*Grant number: N00014-04-1-0607*

**Principal Investigator**

Moeness Amin

**Contributors**

Prof. Moeness Amin

Dr. Wei Sun

Mr. Liyu Liu

**DISTRIBUTION STATEMENT A**  
Approved for Public Release  
Distribution Unlimited

**September 2005**

**20050919 030**

# Table of Contents

Executive Summary.....	2
List of Publications .....	4
<b>Chapter 1</b> A Novel Interference Suppression Scheme for Global Navigation Satellite Systems Using Antenna Array .....	5
1. Introduction.....	5
2. Overview of SCORE Algorithms .....	9
3. Proposed Anti-Jamming GNSS Scheme .....	10
4. Covariance Matrix Estimations .....	17
5. Numerical Results .....	20
6. Conclusions.....	25
Appendix A Mean Calculation .....	26
Appendix B Variance Calculation .....	29
References.....	31
Figures.....	35
<b>Chapter 2</b> Performance Analysis of GPS Receivers in Non-Gaussian Noise Incorporating Precorrelation Filtering and Sampling Rate.....	42
1. Introduction.....	42
2. Non-Gaussian Noise Models .....	44
3. Sampling and Filtering Effects .....	47
4. GPS DLL Performance under Different Noise Sources .....	50
5. Simulation Results .....	55
6. Conclusions.....	56
APPENDIX A.....	56
References.....	60
Tables and Figures .....	63

# Array Processing for Interference Suppression in GPS Receivers

## Executive Summary

This report presents research work performed under the contract no. N00014-04-1-0607 with the Office of Naval Research over the period of May 2004 to September 2005. It includes contributions from Prof. Moeness Amin (PI), Dr. Wei Sun (Postdoctoral Fellow), and Mr. Liyu Liu (graduate Student). The report consists of two chapters. Each chapter has its own abstract and introduction, and has also its own equation numbers, figure numbers, and references.

In Chapter 1, we consider interference suppression and multipath mitigation in Global Navigation Satellite Systems (GNSSs). In particular, a self-coherence anti-jamming scheme is introduced which relies on the unique structure of the coarse/acquisition (C/A) code of the satellite signals. Because of the repetition of the C/A-code within each navigation symbol, the satellite signals exhibit strong self-coherence between chip-rate samples separated by integer multiples of the spreading gain. The proposed scheme utilizes this inherent self-coherence property to excise interferers that have different temporal structures from that of the satellite signals. Using a multiantenna navigation receiver, the proposed approach obtains the optimal set of beamforming coefficients by maximizing the cross correlation between the output signal and a reference signal, which is generated from the received data. It is demonstrated that the proposed scheme can provide high gains toward all satellites in the field of view, while suppressing strong interferers. By imposing constraints on the beamformer, the proposed method is also capable of mitigating multipath that enters the receiver from or near the horizon. No knowledge of either the transmitted navigation symbols or the satellite positions is required.

In Chapter 2, we study the performance of the delay lock loops (DLL) in Global Positioning Systems (GPS) receivers in the presence of non-Gaussian noise. GPS receivers find growing applications in indoor and outdoor communication environments including urban and rural areas. Interference and noise sources for GPS receivers may assume Gaussian or non-Gaussian distributions, specifically when operating inside buildings. The GPS receiver performance under Gaussian additive noise has been extensively studied. Non-Gaussian noise may equally contaminate the GPS satellite signals and compromise the receiver delay lock loops (DLL), producing significant tracking errors. These sources include impulsive noise, ultra-wideband (UWB) signals, and impulse and noise radar signals for target tracking and through-the-wall imaging applications. This chapter considers non-Gaussian noise and examines its effect on GPS correlation and discriminator outputs for the commercial GPS using Coarse Acquisition (C/A) code. The correlator noise output components are produced from the correlation between the noise sequence and the early, late, and punctual reference C/A code. Due to the long time-averaging performed in the GPS correlation loops, these components assume Gaussian distributions. The discriminator tracking error variance is derived, incorporating the effect of noise, the front-end precorrelation filter, and the sampling rate.

## List of Publications

- [1] W. Sun and M. G. Amin, "A self-coherence anti-jamming GPS receiver," IEEE Transactions on Signal Processing, October 2005.
- [2] M. G. Amin and W. Sun, "A novel interference suppression scheme for global navigation satellite systems using antenna arrays," IEEE Journal on Selected Areas in Communications, May 2005.
- [3] M. G. Amin, W. Sun, and A. Lindsey, "Adaptive arrays for GPS receivers," M. Ibnkahla, Editor, in Signal Processing for Mobile Communications Handbook, CRC Press, 2004.
- [4] L. Liu and M. G. Amin, "Performance analysis of GPS receivers in impulsive noise", Proceedings of SPIE Defense & Security Symposium on Digital Wireless Communications VII, Orlando, Florida USA, vol. 5819, March 28-April 1, 2005.
- [5] L. Liu and M. G. Amin, "Noise Analysis of GPS Synchronization Loops", Proceedings of Intelligent Ship Symposium VI on Intelligent Technologies, Villanova, PA, June 1-2, 2005.
- [6] W. Sun and M. G. Amin, "Maximum signal-to-noise ratio GPS anti-jam receiver with subspace tracking," Proceedings of the IEEE International Conference on Acoustics, Speech, and Signal Processing, Philadelphia, PA, March 2005.

# Chapter 1

## A Novel Interference Suppression Scheme for Global Navigation Satellite Systems Using Antenna Array

### 1. Introduction

Satellite navigation is a tool to determine position, velocity, and precise time world wide. A navigation receiving device determines its three dimensional position plus time by measuring the signal traveling time from the satellite to the receiver (the so called *pseudorange* due to the clock offset at the receiver) [1]. The generic name of the satellite navigation systems is Global Navigation Satellite System (GNSS). Currently, there are two operative navigation systems, one is Global Positioning System (GPS) of the United States and the other one is Global Navigation Satellite System (GLONASS) of Russia [2].

Both GPS and GLONASS employ direct sequence spread spectrum (DS SS) signaling. The GPS satellites transmit signals at two  $L$  band frequencies:  $L1 = 1.57542\text{GHz}$  and  $L2 = 1.2276\text{GHz}$ . Each satellite broadcasts two different pseudorandom (PRN) codes, a coarse/acquisition (C/A) code and a precision (P) code, using code division multiple access (CDMA) technique. The  $L1$  carrier transmits both the C/A code and the P code, whereas the  $L2$  carrier only transmits the P code [1]. The GPS C/A code is a Gold code with a chip rate of 1.023 Mchips/sec (or code period 1023) and repeats every millisecond, and the P code, usually encrypted for military use, has a chip rate 10.23 Mchips/sec and repeats about every week. Similar to GPS, GLONASS also has two DS SS components. However, frequency division multiple access (FDMA) technique is used in GLONASS, where each satellite transmits on a different center frequency. The C/A code of GLONASS has a length of 511 chips at a chip rate of 511 kHz, and it is the same for every GLONASS satellite. The C/A code repeats 10 times within each navigation symbol which has a rate of 100 bps. Another component of GLONASS has 10 times the chip rate (5.11 MHz) of

the C/A code and uses a longer PRN code. In this chapter, we consider only the signals induced by the C/A code.

Despite the ever increasing civilian applications, the main drawback of the satellite navigation systems remains to be its high sensibility to interference and multipath [3], [4], [5], [6], [7], [8], which are the two main sources of errors in range and position estimations. The effect of interference on the GNSS receiver is to reduce the signal to noise ratio (SNR) of the navigation signal such that the receiver is unable to obtain measurements from the satellite, thus losing its ability to navigate [1]. Jammers reported to impact the GPS receivers are wideband noise, CW, pulsed noise, pulsed CW, swept tone (chirped), frequency hopping, and spoofers. Each type of jammers has advantages and drawbacks in terms of complexity and effectiveness [9]. The spread spectrum (SS) scheme, which underlines the GNSS signal structure, provides a certain degree of protection against interference. However, when the interferer power becomes much stronger than the signal power, the spreading gain alone is insufficient to yield any meaningful information. For example, for the GPS C/A signal, the receiver is vulnerable to strong interferers whose power exceeds the approximately 30 dB gain ( $10 \log_{10} 1023 \approx 30$  dB) offered via the spreading/despreading process. It is thus desirable that the GNSS receivers operate efficiently in the presence of strong interference, whether it is intentional or unintentional.

Interference suppression in SS communication systems has been an active research topic for many years and a number of techniques have been developed (see, e.g., [4], [10], [11], [12], and references therein). In satellite navigation, interference can be combated in the time, space, or frequency domain, or in a domain of joint variables, e.g., time frequency [13], [14] or space time [15], [16]. Multiple antenna receivers allow the implementations of spatial nulling and beamsteering based on adaptive beamforming and high resolution direction finding methods. These methods are considered to be effective tools for anti jam GPS [9].

Conventional antenna arrays, which are only based on spatial processing, are among the simplest, and yet effective, techniques for narrowband interference suppression. Such techniques, however, is

inadequate for broadband jammers (such as spoofer) cancellation or in the presence of multipath. In these cases, the temporal degree of freedom is required. Space time processing provides the receiver with spatial and temporal selectivity. The spatial selectivity allows the discrimination between the navigation and interference signals based on their respective direction of arrivals (DOA's) [17], [18], [19], [20]. The temporal selectivity is used for broadband interference and multipath cancellation. Generally, the criteria for determining the optimal array weights include maximum signal to interference plus noise ratio (MSINR), minimum mean square error (MMSE), and minimum output power (MOP) [16]. The MSINR approach seeks the array weight vector by maximizing the receiver output SINR. The MMSE method chooses the weight vector such that the mean square difference between the array output and the desired temporal signal is minimized. Since the navigation signal power is well below the noise floor at the receiver, minimizing the output power while attempting to preserve the navigation signal is the goal of the MOP based scheme. While these methods are widely used in interference suppression in satellite navigation systems, one obvious drawback is that they all require some kind of *a priori* knowledge of the problem parameter values. For example, satellite locations are needed in order to calculate the signal power for the MSINR and MMSE methods. In [21], spatial and temporal processing techniques are applied to remove GPS like broadband jammers and recover the navigation information. The assumptions made in [21] are that the chip and bit synchronizations are achieved, implying that pseudorange measurements are obtained. However, the assumption of satellite positions or acquisitions is difficult to enforce under persistent jamming, or during the initial satellite searching stage when any synchronization is yet to be established.

In addition to interference, GPS pseudorange and carrier phase measurements also suffer from a variety of systematic biases, including satellite orbit prediction error and clock drift, ionospheric and tropospheric delay, GPS receiver clock offset, and signal multipath [22]. The satellite orbit and timing, ionospheric, and tropospheric errors can be removed by differencing techniques or significantly reduced by modeling [1]. The receiver clock offset can also be corrected by differencing but is often solved for as an unknown in the position solution. Multipath, on the other hand, is normally uncorrelated between

antenna locations. As a result, differencing will not cancel the errors caused by multipath. Also, modeling multipath for each antenna location is difficult and impractical [23]. To combat signal multipath, many techniques have been proposed. Among them, narrow correlator is one of the most widely used approaches that improves the C/A code tracking performance by reducing the space between the early and late correlator [24]. Other multipath mitigation techniques include multipath elimination delay lock loop (MEDLL) [25] and multipath estimation technology (MET) [22], etc.

This chapter proposes a new interference suppression technique for GNSS using spatial processing, but incorporating the known temporal structure of the C/A signal. A careful examination of the existing interference cancellation techniques reveals that, though efficient in most situations, they do not fully take advantage of the unique C/A signal structure, namely the replication of the C/A code. Due to the repetition of the spreading code, the GNSS C/A signal exhibits strong self coherence between chip samples that are separated by integer multiples of the spreading gain. Utilizing this feature, an anti jamming technique is developed to suppress a large class of narrowband and broadband interferers. It also has the capability of mitigating multipath, resulting in improved accuracy in pseudorange measurements. The proposed technique allows the civilian C/A code tracking and acquisition operations in the presence of strong interference, specifically at “cold start”, where there is no prior information on satellite angular positions or ranges [26]. In military applications, the encrypted P code is used instead of the C/A code. However, due to the short duration of the P code chip (10 times shorter than the C/A code chip), the synchronization in P code is usually difficult to achieve using the early late correlator, and assistance from the C/A code is needed [24]. With the receiver introduced in this chapter, initial synchronization in the P code can be established by first processing the interference suppressed C/A code. In essence, the self coherence based anti jamming approach is a blind technique, which does not require the knowledge of the navigation data or satellite locations to perform interference suppression. This makes it most applicable in the initial satellite searching phase when such information is unavailable, or in a prolonged jamming environment where the formerly obtained satellite positions are no longer reliable.

The rest of the chapter is organized as follows. In Section 2, we briefly review the concept of spectral self coherence restoral. An anti jamming GNSS scheme is presented in Section 3 and two receivers based on such scheme are developed. In Section 4, we discuss various important issues related to the performance of the proposed GPS receiver. Numerical results are presented in Section 5 to demonstrate the performance of the proposed receiver. Finally, Section 6 concludes this section.

## 2. Overview of SCORE Algorithms

The proposed anti jamming GNSS technique builds on the basic concept of the self coherence restoral algorithm proposed in [27]. A signal  $s(t)$  is referred to as spectrally self coherent at frequency separation  $\beta$  if the correlation between the signal and its frequency shifted version is nonzero for some lag  $\tau$ , i.e., if [27], [28]

$$\rho_{ss}^{(\beta)}(\tau) = \frac{\left\langle s(t)s^*(t-\tau)e^{-j2\pi\beta t} \right\rangle_{\infty}}{\sqrt{\left\langle |s(t)|^2 \right\rangle_{\infty} \left\langle |s^*(t-\tau)e^{-j2\pi\beta t}|^2 \right\rangle_{\infty}}} = \frac{R_{ss}^{(\beta)}(\tau)}{R_{ss}(\tau)} \neq 0 \quad (0.1)$$

where  $(\cdot)^*$  denotes the complex conjugate and  $\langle \cdot \rangle_{\infty}$  represents the infinite time averaging operation.  $\rho_{ss}^{(\beta)}(\tau)$  is the *self-coherence function* and  $R_{ss}(0)$  and  $R_{ss}^{(\beta)}(\tau)$  represent the average power and *cyclic autocorrelation function* of  $s(t)$ , respectively. For an  $M$ -element vector waveform  $\mathbf{x}(t)$ , the *cyclic autocorrelation matrix*  $\mathbf{R}_{ss}^{(\beta)}(\tau)$  is defined as

$$\mathbf{R}_{ss}^{(\beta)}(\tau) \triangleq \left\langle \mathbf{x}(t)\mathbf{x}^H(t-\tau)e^{-j2\pi\beta t} \right\rangle_{\infty} \quad (0.2)$$

where  $(\cdot)^H$  stands for the complex conjugate transpose. Complex wide sense cyclostationary waveforms exhibit spectral self coherence at discrete multiples of the time periodicities of the waveform statistics [27]. The signal waveforms that possess the self coherence feature include most communication signals, such as PCM signals and BPSK signals [28].

The spectral self coherence restoral (SCORE) beamforming techniques have been shown to blindly extract the desired signal in the presence of unknown noise and interference [27]. The SCORE algorithms seek the beamformer weight vector that maximizes a measure of the cyclic feature of the beamformer output. For example, in the presence of interference, the received signal is given by  $x(t) = as(t) + v(t)$ , where  $a$  is the signal amplitude and  $v(t)$  is the interference, which is assumed to be independent of  $s(t)$ . If  $s(t)$  is spectrally self coherent at a frequency shift  $\beta$ , then the cyclic autocorrelation of  $x(t)$  can be expressed as [27]

$$R_{xx}^{(\beta)}(\tau) = |a|^2 R_{ss}^{(\beta)}(\tau) + R_{vv}^{(\beta)}(\tau) = |a|^2 R_{ss}^{(\beta)}(\tau) \quad (0.3)$$

Equation (1.3) shows that the shift in frequency completely decorrelates the interference component in  $x(t)$ , given that  $v(t)$  is not spectrally self-coherent at the frequency separation  $\beta$ .

There are several different versions of the SCORE algorithm, of which the least-squares (LS) SCORE is the simplest. The LS-SCORE algorithm determines the array weight vector by minimizing the difference between the array output and a reference signal, which is obtained by processing the delayed and frequency-shifted version of the received signal. Other SCORE algorithms include the cross-SCORE algorithm, which determines the beamformer by strengthening the cross-correlation between the output of the array and a reference signal, and the auto-SCORE algorithm, which maximizes the spectral self-coherence strength at the output of a linear combiner [27]. The self-coherence anti-jamming scheme proposed in this section is based on the cross-SCORE algorithm.

### 3. Proposed Anti-Jamming GNSS Scheme

Before introducing the proposed anti-jamming receiver, we first examine the temporal structure of the navigation signal, as the receiver is developed by exploiting the repetitive feature of the C/A signal. Figure 1 depicts the structure of the received noise-free navigation signal, where the BPSK modulated navigation symbols (simply referred to as “symbol” thereafter) are spread by a PRN code with spreading gain of  $P$  ( $P = 1023$  for GPS and  $P = 511$  for GLONASS) and chip-rate sampled. The code sequence

(denoted as “spreading block” in Figure 1) is repeated  $L$  times ( $L = 20$  for GPS and  $L = 10$  for GLONASS) within each symbol. Two blocks of data are formed at the receiver: a *data block*, which spans  $N$  consecutive samples, and a *reference block* with the same number of samples as the data block. The distance between the respective samples in the data and reference blocks is set equal to  $jP$  chips, where  $1 \leq j < L$ . Obviously, due to the repetition of the spreading code, the  $n$ th sample in the data block will have the same value as the corresponding  $n$ th sample in the reference block, providing that the two samples belong to the same symbol.

From the temporal structure of the C/A signal, we observe the inherent self-coherence between samples in the data block and the reference block, due to the repetition of the spreading code. Based on this observation, a novel anti-jamming technique is developed in this section, and Figure 2 shows a block diagram of the proposed receiver with this technique. In Figure 2, an  $M$ -element array is deployed. There are two beamformers in the receiver: a main beamformer  $\mathbf{w}$ , processing samples in the data block, and an auxiliary beamformer  $\mathbf{f}$ , handling data from the reference block. An error signal  $e(t)$  is formed as the difference between the beamformer output  $z(t)$  and a reference signal  $d(t)$ , which is the output of  $\mathbf{f}$ . For the proposed scheme, the weight vectors  $\mathbf{w}$  and  $\mathbf{f}$  are updated according to the cross-SCORE algorithm. The signal reaching the GNSS receiver is the aggregate of the satellite navigation signals, their respective multipaths, additive white Gaussian noise (AWGN), and broadband/narrowband interferers. Thus, after carrier synchronization, the signal received at the receiver can be expressed as

$$\begin{aligned} \mathbf{x}(n) &= \sum_{q=0}^Q s_q(nT_s - \tau_q) \mathbf{a}_q e^{j\phi_q} + \sum_{k=1}^K B_k u_k(n) \mathbf{d}_k + \mathbf{v}(n) \\ &= s_0(nT_s - \tau_0) \mathbf{a}_0 e^{j\phi_0} + \sum_{q=1}^Q s_q(nT_s - \tau_q) \mathbf{a}_q e^{j\phi_q} + \sum_{k=1}^K B_k u_k(n) \mathbf{d}_k + \mathbf{v}(n) \end{aligned} \quad (0.4)$$

where  $T_s$  is the Nyquist sampling interval,  $Q$  is the number of multipath components, with subscript 0 designated to the direct-path signal. Due to the weak cross-correlation of the C/A-codes, only one satellite is considered in Equation (1.4). In the above equation,  $s_q(n)$ ,  $\tau_q$ , and  $\phi_q$  are the signal sample, time-delay, and phase-shift of the  $q$ th multipath component, respectively,  $K$  is the number of interferers,  $u_k(n)$

is the waveform of the  $k$ th interferer with amplitude  $B_k$ . The vectors  $\mathbf{a}_q$  and  $\mathbf{d}_k$  are, respectively,  $M \times 1$  spatial signatures of the  $q$ th satellite multipath and the  $k$ th interferer, and  $\mathbf{v}(n)$  consists of noise samples.

Let  $s(n) \square s_0(nT_s - \tau_0)\mathbf{a}_0 e^{j\phi_0}$  denote the data vector across the array due to the direct-path signal. Then,

Equation (1.4) can be rewritten as

$$\mathbf{x}(n) = \mathbf{s}(n) + \tilde{\mathbf{s}}(n) + \mathbf{u}(n) + \mathbf{v}(n) \quad (0.5)$$

where  $\tilde{\mathbf{s}}(n) \square \sum_{q=1}^Q s_q(nT_s - \tau_q)\mathbf{a}_q e^{j\phi_q}$  and  $\mathbf{u}(n) \square \sum_{k=1}^K B_k u_k(n)\mathbf{d}_k$ . Assuming a direct-path to the satellite at

direction  $\mu$  and a uniform linear array, we can express vector  $\mathbf{a}_0$  in the specific format of a steering vector as

$$\mathbf{a}_0 = \mathbf{a}(\theta) \square \left[ 1, e^{j2\pi f_c \tau}, \dots, e^{j2\pi f_c (M-1)\tau} \right]^T \quad (0.6)$$

where  $f_c$  is the carrier frequency,  $\tau = \Delta / c \sin \theta$  is the interelement path delay of the source in the direction of  $\theta$ ,  $c$  is the propagation speed of the waveform, and  $\Delta$  is the sensor spacing. According to the formulation of the data and reference blocks, the counterpart of  $\mathbf{x}(n)$  in the reference block within the same symbol can be written as

$$\begin{aligned} \mathbf{x}(n - jP) &= \sum_{q=0}^Q s_q(nT_s - \tau_q - jP)\mathbf{a}_q e^{j\phi_q} + \sum_{k=1}^K B_k u_k(n - jP)\mathbf{d}_k + \mathbf{v}(n - jP) \\ &= \sum_{q=0}^Q s_q(nT_s - \tau_q)\mathbf{a}_q e^{j\phi_q} + \sum_{k=1}^K B_k u_k(n - jP)\mathbf{d}_k + \mathbf{v}(n - jP) \\ &= \mathbf{s}(n) + \tilde{\mathbf{s}}(n) + \mathbf{u}(n - jP) + \mathbf{v}(n - jP) \end{aligned} \quad (0.7)$$

where we have assumed that, when considered within the same symbol,

$$s_q(nT_s - \tau_q) = s_q(nT_s - \tau_q - jP), \quad q = 0, \dots, Q \quad (0.8)$$

Compared to the general case of self-coherence, there is no frequency difference between the signal samples in the data and reference blocks, i.e., the frequency shift  $\beta = 0$ .

From Figure 2, the beamformer output and the reference signal are given by  $z(n) \square \mathbf{w}^H \mathbf{x}(n)$  and  $d(n) \square \mathbf{f}^H \mathbf{x}(n - jP)$ , respectively. We define the following covariances:

$$R_{zd} \square E \{ z(n) d^H(n) \} = \mathbf{w}^H E \{ \mathbf{x}(n) \mathbf{x}^H(n - jP) \} \mathbf{f} \quad (0.9)$$

$$R_{zz} \square E \{ z(n) z^H(n) \} = \mathbf{w}^H E \{ \mathbf{x}(n) \mathbf{x}^H(n) \} \mathbf{w} \quad (0.10)$$

$$R_{dd} \square E \{ d(n) d^H(n) \} = \mathbf{f}^H E \{ \mathbf{x}(n - jP) \mathbf{x}^H(n - jP) \} \mathbf{f} \quad (0.11)$$

Under the assumption that the navigation signal, interference, and noise are independent, then

$$\mathbf{R}_{xx} \square E \{ \mathbf{x}(n) \mathbf{x}^H(n) \} = E \{ \mathbf{x}(n - jP) \mathbf{x}^H(n - jP) \} = \mathbf{R}_s + \mathbf{R}_u + \mathbf{R}_v \quad (0.12)$$

The three terms on the right-hand side of Equation (0.12) denote, respectively, the covariance matrices of the C/A signal, including both the direct-path and multipath signals, interference, and noise:

$$\mathbf{R}_s \square E \{ [\mathbf{s}(n) + \tilde{\mathbf{s}}(n)] [\mathbf{s}(n) + \tilde{\mathbf{s}}(n)]^H \}, \quad \mathbf{R}_u \square E \{ \mathbf{u}(n) \mathbf{u}^H(n) \}, \quad \text{and} \quad \mathbf{R}_v \square E \{ \mathbf{v}(n) \mathbf{v}^H(n) \}.$$

If the navigation signal is the only data component which correlates with its delayed version, then the cross-correlation matrix between the corresponding data vectors in the data and reference blocks simplifies to [cf. Equation (0.3)]

$$\mathbf{R}_{xx}^{(P)} \square E \{ \mathbf{x}(n) \mathbf{x}^H(n - jP) \} = \mathbf{R}_s \quad (0.13)$$

### 3.1. Cross-SCORE Algorithm Based Receiver

We first consider the receiver design by directly applying the cross-SCORE algorithm. For the proposed GNSS anti-jamming scheme, there are two beamformers  $\mathbf{w}$  and  $\mathbf{f}$  to be determined. With  $d(n)$  serving as the reference signal, we define  $e(n) \square z(n) - d(n)$  as the difference between the receiver's output and the reference signal. The relationship between  $\mathbf{w}$  and  $\mathbf{f}$  can be established in the least-squares (LS) sense.

For a fixed beamformer  $\mathbf{w}$ , the LS solution of  $\mathbf{f}$  is given by  $\mathbf{f}_{LS} = \mathbf{R}_{xx}^{-1} \mathbf{r}_{xx}$ , where

$$\mathbf{r}_{xx} = E \{ \mathbf{x}(n - jP) z^H(n) \} = \mathbf{R}_{xx}^{(P)H} \mathbf{w}. \quad \text{Similarly, if } \mathbf{f} \text{ is fixed, then } \mathbf{w}_{LS} = \mathbf{R}_{xx}^{-1} \mathbf{R}_{xx}^{(P)H} \mathbf{f}.$$

According to the cross-SCORE algorithm, the beamformers  $\mathbf{w}$  and  $\mathbf{f}$  are obtained by maximizing the cross-correlation between  $z(n)$  and  $d(n)$ :

$$C(\mathbf{w}, \mathbf{f}) \propto \frac{|R_{zd}|^2}{R_{zz}R_{dd}} = \frac{|\mathbf{w}^H \mathbf{R}_{xx}^{(P)} \mathbf{f}|^2}{[\mathbf{w}^H \mathbf{R}_{xx} \mathbf{w}][\mathbf{f}^H \mathbf{R}_{xx} \mathbf{f}]} \quad (0.14)$$

Substituting  $\mathbf{f}$  and  $\mathbf{w}$  in the above equation by  $\mathbf{f}_{LS}$  and  $\mathbf{w}_{LS}$ , respectively, we have

$$C(\mathbf{w}, \mathbf{f}_{LS}) = \frac{\mathbf{w}^H \mathbf{R}_{xx}^{(P)} \mathbf{R}_{xx}^{-1} \mathbf{R}_{xx}^{(P)} \mathbf{w}}{\mathbf{w}^H \mathbf{R}_{xx} \mathbf{w}} \quad (0.15)$$

$$C(\mathbf{w}_{LS}, \mathbf{f}) = \frac{\mathbf{f}^H \mathbf{R}_{xx}^{(P)} \mathbf{R}_{xx}^{-1} \mathbf{R}_{xx}^{(P)} \mathbf{f}}{\mathbf{f}^H \mathbf{R}_{xx} \mathbf{f}} \quad (0.16)$$

The weight vectors  $\mathbf{w}$  and  $\mathbf{f}$  that maximize  $C(\mathbf{w}, \mathbf{f}_{LS})$  and  $C(\mathbf{w}_{LS}, \mathbf{f})$ , respectively, are readily shown to be the eigenvectors corresponding to the largest eigenvalues of the generalized eigenvalue problems:

$$\mathbf{R}_{xx} \mathbf{w} = \lambda \mathbf{R}_{xx}^{(P)} \mathbf{R}_{xx}^{-1} \mathbf{R}_{xx}^{(P)} \mathbf{w} \quad (0.17)$$

$$\mathbf{R}_{xx} \mathbf{f} = \kappa \mathbf{R}_{xx}^{(P)} \mathbf{R}_{xx}^{-1} \mathbf{R}_{xx}^{(P)} \mathbf{f} \quad (0.18)$$

where  $\lambda$  and  $\kappa$  are the eigenvalues.

It is observed from Equations (0.17) and (1.18) that, for the proposed receiver, the main beamformer  $\mathbf{w}$ , which generates the receiver outputs, is equivalent to the auxiliary beamformer  $\mathbf{f}$  that provides the reference signal. This equivalence, however, is not surprising because of the unique structure of the C/A signal. From Equations (0.4) and (1.7), we note that the self-coherence of the navigation signal is due to the time lag between the two samples which do not encounter any frequency shift after the frequency demodulation. Therefore,  $\mathbf{x}(n)$  and  $\mathbf{x}(n-jP)$  have the same correlation function, given by Equation (1.11). For the general case of self-coherence, on the other hand, the signal auto-correlation function does not necessarily equal to the auto-correlation function of the frequency-shifted, time-lagged version of the original signal. As a result, the cross-SCORE algorithm will not produce two identical beamformers [27], as it does for the proposed receiver.

Simulations presented in Section V show that the cross-SCORE based receiver performs fairly well in a jamming environment. It is capable of producing high gains for satellites currently in the field of view, while suppressing strong jammers. However, such a receiver provides no measures against multipath, which is one of the dominant error sources in navigation. To address the multipath issue, we modify the receiver design, as discussed in the next subsection.

### 3.2. Modified Cross-SCORE Algorithm Based Receiver

Since the GNSS signal multipath shares the same structure as the direct-path signal, it is expected that both the C/A signal and the undesired multipath components will appear at the receiver's output undistorted.

It is known that the satellites typically lie above the horizon, whereas the multipath is often generated from local scatters near the horizon [16]. To equip the receiver with means to combat multipath, while maintaining the self-coherent approach, we introduce constraints on  $\mathbf{f}$  such that the reference signal  $d(n)$  does not contain reflections from near the horizon. To do so, we define equally spaced directions  $\gamma_d$ ,  $d=1, \dots, D$ , covering some solid angle  $\Omega$  near the horizon. Let  $\mathbf{B} = [\mathbf{b}(\gamma_1) \ \dots \ \mathbf{b}(\gamma_D)]$  be the  $M \times D$  matrix consisting of steering vectors defined as in Equation (6). To mitigate multipath in the range  $\Omega$ , we require  $\mathbf{B}^H \mathbf{f} = \mathbf{0}$ . Then, the cost function in Equation (1.16) is rewritten as

$$\mathbf{f}_{\text{opt}} = \arg \max_{\mathbf{f}} \frac{\mathbf{f}^H \tilde{\mathbf{R}}_{xx} \mathbf{f}}{\mathbf{f}^H \mathbf{R}_{xx} \mathbf{f}}, \text{ subject to } \mathbf{B}^H \mathbf{f} = \mathbf{0} \quad (0.19)$$

where  $\tilde{\mathbf{R}}_{xx} = \mathbf{R}_{xx}^{(P)} \mathbf{R}_{xx}^{-1} \mathbf{R}_{xx}^{(P)H}$ . The solution of the above equation is obtained as follows. Let  $r = \text{rank}(\mathbf{B}) \leq \min(M, D)$  be the rank of the  $\mathbf{B}$  matrix. Performing the singular value decomposition (SVD) [29] of  $\mathbf{B}$  yields

$$\mathbf{U}^H \mathbf{B}^H \mathbf{V} = \begin{bmatrix} \Lambda & \mathbf{0} \\ \mathbf{0} & \mathbf{0} \end{bmatrix} \quad (0.20)$$

where  $\mathbf{U}$  and  $\mathbf{V}$  are two unitary matrices with dimension  $M \times M$  and  $D \times D$ , respectively, and

$$\Lambda = \text{diag}\{\sigma_1, \sigma_2, \dots, \sigma_r\} \quad (0.21)$$

where  $\sigma_1 \geq \sigma_2 \geq \dots \geq \sigma_r$  are eigenvalues of  $\mathbf{B}$  arranged in a decreasing order. Let  $\mathbf{A}$  be formed from the last  $M-r$  columns of  $\mathbf{U}$ . Thus,  $\mathbf{A}$  spans the null space of  $\mathbf{B}^H$ , i.e.,  $\mathbf{B}^H \mathbf{A} = \mathbf{0}$ . Let  $\boldsymbol{\alpha}$  be a  $(M-r) \times 1$  vector such that

$$\mathbf{f} = \mathbf{A}\boldsymbol{\alpha} \quad (0.22)$$

Using vector  $\boldsymbol{\alpha}$ , the constrained maximization problem in Equation (1.19) is transformed to an unconstrained one:

$$\boldsymbol{\alpha} = \arg \max_{\boldsymbol{\alpha}} \frac{\boldsymbol{\alpha}^H \mathbf{A}^H \tilde{\mathbf{R}}_{xx} \mathbf{A} \boldsymbol{\alpha}}{\boldsymbol{\alpha}^H \mathbf{A}^H \mathbf{R}_{xx} \mathbf{A} \boldsymbol{\alpha}} \quad (0.23)$$

The above generalized eigendecomposition problem can be solved using Cholesky decomposition. Particularly, since  $\mathbf{R}_{xx}$  is positive definite,  $\mathbf{A}^H \mathbf{R}_{xx} \mathbf{A}$  is also positive definite. Then the Cholesky decomposition of  $\mathbf{A}^H \mathbf{R}_{xx} \mathbf{A}$  is  $\mathbf{A}^H \mathbf{R}_{xx} \mathbf{A} = \mathbf{G}\mathbf{G}^H$ , where  $\mathbf{G}$  is a  $(M-r) \times (M-r)$  matrix with full rank [29] and, thus, invertible. Let  $\boldsymbol{\alpha} = \mathbf{G}^{-H} \boldsymbol{\beta}$ . Then

$$\frac{\boldsymbol{\alpha}^H \mathbf{A}^H \tilde{\mathbf{R}}_{xx} \mathbf{A} \boldsymbol{\alpha}}{\boldsymbol{\alpha}^H \mathbf{A}^H \mathbf{R}_{xx} \mathbf{A} \boldsymbol{\alpha}} = \frac{\boldsymbol{\beta}^H \mathbf{G}^{-1} \mathbf{A}^H \tilde{\mathbf{R}}_{xx} \mathbf{A} \mathbf{G}^{-H} \boldsymbol{\beta}}{\boldsymbol{\beta}^H \mathbf{G}^{-1} \mathbf{G} \mathbf{G}^H \mathbf{G}^{-H} \boldsymbol{\beta}} = \frac{\boldsymbol{\beta}^H \mathbf{G}^{-1} \mathbf{A}^H \tilde{\mathbf{R}}_{xx} \mathbf{A} \mathbf{G}^{-H} \boldsymbol{\beta}}{\boldsymbol{\beta}^H \boldsymbol{\beta}} \quad (0.24)$$

Accordingly, the maximization problem becomes

$$\max_{\boldsymbol{\alpha}} \frac{\boldsymbol{\alpha}^H \mathbf{A}^H \tilde{\mathbf{R}}_{xx} \mathbf{A} \boldsymbol{\alpha}}{\boldsymbol{\alpha}^H \mathbf{A}^H \mathbf{R}_{xx} \mathbf{A} \boldsymbol{\alpha}} = \max_{\boldsymbol{\beta}} \frac{\boldsymbol{\beta}^H \mathbf{G}^{-1} \mathbf{A}^H \tilde{\mathbf{R}}_{xx} \mathbf{A} \mathbf{G}^{-H} \boldsymbol{\beta}}{\boldsymbol{\beta}^H \boldsymbol{\beta}} = \max_{\boldsymbol{\beta}} \boldsymbol{\beta}^H \mathbf{G}^{-1} \mathbf{A}^H \tilde{\mathbf{R}}_{xx} \mathbf{A} \mathbf{G}^{-H} \boldsymbol{\beta} \quad (0.25)$$

under the standard constraint  $\|\boldsymbol{\beta}\| = 1$ , where  $\|\cdot\|$  is the vector 2-norm [29]. Hence,  $\boldsymbol{\beta}$  is given by the eigenvector associated with the maximum eigenvalue of  $\mathbf{G}^{-1} \mathbf{A}^H \tilde{\mathbf{R}}_{xx} \mathbf{A} \mathbf{G}^{-H}$ . And, finally,

$$\mathbf{f}_{\text{opt}} = \mathbf{A} \mathbf{G}^{-H} \boldsymbol{\beta} \quad (0.26)$$

The beamformer  $\mathbf{w}$  is derived as

$$\mathbf{w}_{\text{opt}} = \mathbf{R}_{xx}^{-1} \mathbf{R}_{xx}^{(P)} \mathbf{f}_{\text{opt}} = \mathbf{R}_{xx}^{-1} \mathbf{R}_{xx}^{(P)} \mathbf{A} \boldsymbol{\alpha} \quad (0.27)$$

according to the LS relation between  $\mathbf{w}$  and  $\mathbf{f}$ .

## 4. Covariance Matrix Estimations

In practice, the covariance matrices  $\mathbf{R}_{xx}$  and  $\mathbf{R}_{xx}^{(P)}$  are unknown and have to be replaced by their sample estimates. Define the  $M \times N$  data and reference matrices as  $\mathbf{X}_N = [\mathbf{x}(n), \dots, \mathbf{x}(n-(N-1))]$  and  $\mathbf{X}_{Nref} = [\mathbf{x}(n-jP), \dots, \mathbf{x}(n-(N-1)-jP)]$ , where  $N$  is the block length and  $N \leq P$ . The sample covariance matrices are then given by

$$\hat{\mathbf{R}}_{xx} = \frac{1}{N} \mathbf{X}_N \mathbf{X}_N^H \quad (0.28)$$

$$\hat{\mathbf{R}}_{xx}^{(P)} = \frac{1}{N} \mathbf{X}_N \mathbf{X}_{Nref}^H \quad (0.29)$$

And, the beamformers  $\mathbf{w}$  and  $\mathbf{f}$  are calculated correspondingly.

It is noted from Equation (1.16) that the covariance matrices  $\mathbf{R}_{xx}$  and  $\mathbf{R}_{xx}^{(P)}$  determine the performance of the proposed receiver. In practical implementations, the data and reference blocks  $\mathbf{X}_N$  and  $\mathbf{X}_{Nref}$  are used to estimate  $\mathbf{R}_{xx}$  and  $\mathbf{R}_{xx}^{(P)}$ , and subsequently provide the weight vector  $\mathbf{w}$ , which is then applied to process signal samples in the data block. The key assumption made for the proposed GPS receiver in Section III is that both the data and reference samples,  $\mathbf{x}(n)$  and  $\mathbf{x}(n-jP)$ ,  $1 \leq j < 20$ , belong to the same navigation symbol. However, since the data samples used for covariance matrix estimations are selected randomly, and interference suppression is performed prior to any symbol synchronization process, there is no guarantee that the data and reference samples belong to the same symbol. Questions arise as how will the receiver perform when the above assumption fails, i.e., the data and reference samples lie in two adjacent symbols?

To answer the above question, we relax the condition imposed in Section 3, and develop the general expression of the covariance matrices between the data and reference samples,  $\mathbf{x}(n)$  and  $\mathbf{x}(n-jP)$ . Define the following events:

$$\begin{aligned}
A_1 &: \mathbf{x}(n) \text{ \& } \mathbf{x}(n-jP) \text{ are within the same symbol,} \\
A_2 &: \mathbf{x}(n) \text{ \& } \mathbf{x}(n-jP) \text{ are in two adjacent symbols,} \\
A_{21} &: \mathbf{x}(n) \text{ \& } \mathbf{x}(n-jP) \text{ are in two symbols with the same sign,} \\
A_{22} &: \mathbf{x}(n) \text{ \& } \mathbf{x}(n-jP) \text{ are in two symbols with different signs}
\end{aligned} \tag{0.30}$$

With random selection of time  $n$ , and using the repetitive property of the C/A-code, it is straightforward to show that the corresponding probabilities of the above events are

$$\Pr\{A_1\} = \frac{T-jP}{T} = 1 - \frac{jP}{T}, \Pr\{A_2\} = \frac{jP}{T}, \Pr\{A_{21}\} = \frac{jP}{2T}, \text{ and } \Pr\{A_{22}\} = \frac{jP}{2T}, \text{ respectively, where } T$$

$= 20P$  is the total number of samples in one symbol. The exact expression of the cross-correlation

function  $\mathbf{R}_{xx}^{(P)}$  can be written in terms of the above probabilities and conditional expectations as

$$\begin{aligned}
\mathbf{R}_{xx}^{(P)} &= E\{\mathbf{x}(n)\mathbf{x}^H(n-jP)|A_1\}\Pr\{A_1\} + E\{\mathbf{x}(n)\mathbf{x}^H(n-jP)|A_2\}\Pr\{A_2\} \\
&= E\{\mathbf{x}(n)\mathbf{x}^H(n-jP)|A_1\}\Pr\{A_1\} \\
&\quad + E\{\mathbf{x}(n)\mathbf{x}^H(n-jP)|A_{21}\}\Pr\{A_{21}\} + E\{\mathbf{x}(n)\mathbf{x}^H(n-jP)|A_{22}\}\Pr\{A_{22}\}
\end{aligned} \tag{0.31}$$

$$\text{Since } E\{\mathbf{x}(n)\mathbf{x}^H(n-jP)|A_1\} = E\{\mathbf{x}(n)\mathbf{x}^H(n-jP)|A_{21}\} = \mathbf{R}_s, \text{ and}$$

$$E\{\mathbf{x}(n)\mathbf{x}^H(n-jP)|A_{22}\} = -\mathbf{R}_s, \text{ then}$$

$$\mathbf{R}_{xx}^{(P)} = \mathbf{R}_s (\Pr\{A_1\} + \Pr\{A_{21}\}) - \mathbf{R}_s \Pr\{A_{22}\} = \left(1 - \frac{jP}{T}\right) \mathbf{R}_s \tag{0.32}$$

Equation (1.32) shows that the covariance matrix  $\mathbf{R}_{xx}^{(P)}$  depends on the distance between the data and reference samples  $jP$ . The maximum value of  $\mathbf{R}_{xx}^{(P)}$  is achieved when  $j = 1$ , representing the closest possible data and reference blocks.

In practice, however, sample estimates, obtained from Equations (1.27) and (1.28) using the data and reference blocks  $\mathbf{X}_N$  and  $\mathbf{X}_{N_{\text{ref}}}$ , replace the exact values in Equation (1.32). It can be readily shown that if  $\mathbf{X}_N$  and  $\mathbf{X}_{N_{\text{ref}}}$  are  $jP$  samples apart,  $1 \leq j < 20$ , the probability of the two blocks belonging to the same symbol or, equivalently, in two adjacent symbols with the same sign, is  $1 - \frac{jP + N}{2T}$ . On the other hand, the probability that  $\mathbf{X}_N$  and  $\mathbf{X}_{N_{\text{ref}}}$  are in two adjacent symbols with opposite signs is  $\frac{jP - N}{2T}$ . Using the

above probabilities, the expected values of  $\hat{\mathbf{R}}_{xx}$  and  $\hat{\mathbf{R}}_{xx}^{(P)}$  are derived in Appendix A as:

$$\overline{\hat{\mathbf{R}}_{xx}} = \mathbf{R}_s + \mathbf{R}_u + \mathbf{R}_v, \quad (0.33)$$

$$\overline{\hat{\mathbf{R}}_{xx}^{(P)}} = \left(1 - \frac{jP}{T}\right) \mathbf{R}_s, \quad (0.34)$$

which show the same dependency on  $jP$  as in Equation (1.32) and that  $\hat{\mathbf{R}}_{xx}$  and  $\hat{\mathbf{R}}_{xx}^{(P)}$  are unbiased estimates of  $\mathbf{R}_{xx}$  and  $\mathbf{R}_{xx}^{(P)}$ , respectively.

The above covariance matrix estimations use only one data block and its replicated reference block. To fully take advantage of the repetitive feature of the C/A-code, multiple data/reference blocks can be used in the time-averaging. Particularly, using  $G$  data and reference blocks, Equations (1.27) and (1.28), respectively, become

$$\hat{\mathbf{R}}_{xxG} = \frac{1}{G} \sum_{g=1}^G \mathbf{X}_N(g) \mathbf{X}_N^H(g) / N \quad (0.35)$$

$$\hat{\mathbf{R}}_{xxG}^{(P)} = \frac{1}{G} \sum_{g=1}^G \mathbf{X}_N(g) \mathbf{X}_{N_{\text{ref}}}^H(g) / N \quad (0.36)$$

In the case when one of the data blocks (and, respectively, a reference block) is split between two adjacent symbols with opposite signs, a maximum of only two of the  $G$  terms in the above equation may suffer from symbol transition, whereas the rest of the terms will be coherently combined. Appendix A and B derive the mean and variance of the above estimations, showing the value of using a higher value of  $G$ .

## 5. Numerical Results

In this section, we evaluate the performance of the proposed self-coherence anti-jamming receiver using the GPS C/A signals.

A uniform linear array (ULA) consisting of  $M = 7$  sensors with half-wavelength spacing is used in simulations with one satellite and no multipath. We set  $M = 11$  for simulations with multiple satellites or multipath. The GPS navigation symbols are in the BPSK format and spread by C/A-codes (Gold codes) with processing gain of  $P = 1023$ . We select the first satellite C/A-code for concept demonstration. At the receiver, chip-rate sampling is performed and  $N = 800$  samples are collected in both the data and reference blocks for covariance matrix estimations. The signal-to-noise ratio (SNR) and signal-to-interference-plus-noise ratio (SINR) are defined, respectively, as  $\text{SNR} = 10\log_{10} 1/P_v$  and  $\text{SINR} = 10\log_{10} 1/(P_i + P_v)$ , all in dB, where unit signal power is assumed for simplicity,  $P_v$  is the noise power, and  $P_i$  is the interference power. The jammer-to-signal ratio (JSR) is defined as  $\text{JSR} = 10\log_{10} P_i$  dB. Interferers used in the simulations are generated as broadband binary signals having the same rates as the C/A-codes, but with a different structure than that of the C/A signals.

### 5.1. Antenna Beam Pattern without Interference

We first consider the scenarios in which no interference presents at the receiver. SNR is -30 dB. Covariance matrices are estimated using one data block and one reference block taken within the same symbol. The performance of the cross-SCORE based receiver is shown in Figure 3, where the antenna pattern is formed towards the satellite located at  $\theta = 30^\circ$ .

We recall the discussions in Section 4 which suggest that better performance can be expected when multiple data and reference blocks are used to estimate the covariance matrices. In Appendix B, the variances of the sample estimates of  $\mathbf{R}_{xxG}^{(P)}$  are calculated and it shows that using multiple data/reference blocks can indeed reduce the estimation variance. We now demonstrate experimentally the effect of

multi-block estimation on the receiver performance. Particularly, a very special situation is created where one of the data blocks is evenly split between two symbols having opposite signs. SNR is set at -40 dB. If  $G = 2$  and the split data block happens to be the second one, the receiver fails to provide any substantial gain for the satellite located at  $30^\circ$ , as shown in Figure 4(a). This is because that elements in the time-averaging of  $\hat{\mathbf{R}}_{xxG}^{(P)}$  given by Equation (0.35) cancel each other, resulting in significantly weak cross-correlation between  $z(n)$  and  $d(n)$  [cf. Equation (0.14)]. If, on the other hand,  $G > 2$  data and reference blocks are involved in the estimation, the split of one block will not have such a dramatic impact on the receiver performance as in the  $G = 2$  case, as only two among  $G$  blocks are affected due to the split. It is clear from Figure 4(b) that a beam is generated towards the satellite with  $G = 7$  despite the split. Generally, to avoid the performance degradation, it is recommended that odd number of samples ( $N$ ) should be chosen for each data/reference block and  $2 < G < D$ .

It is known that in satellite navigation, at least four satellites are needed simultaneously in the field of view in order to calculate the receiver's three-dimensional position and time. Since the proposed receiver relies on the special structure of the C/A signals to suppress interference and all satellite emitted C/A signals share the same repetitive feature, it is expected that the receiver will pass the signals from all satellites with high gains. In the simulation, the satellites are located at  $\theta_1 = 10^\circ$ ,  $\theta_2 = 30^\circ$ ,  $\theta_3 = 50^\circ$ , and  $\theta_4 = 70^\circ$ , with SNR = -30 dB. As shown in Figure 5, four clear beams are generated towards the four satellites.

A point worth mentioning is that the receiver presented in this section is able to suppress interference for all satellites at once. In GNSS, since the satellite spreading codes are known at the receiver, it may be intuitive to consider using the spreading code as the reference instead of generating one from the received data. Even though the locally generated spreading code is noise and interference free, it cannot serve as the reference signal in the proposed receiver because 1) the alignment of the incoming signal and the local reference code may not be established during the interference removal stage, hence there is no guarantee that the data block and reference blocks are separated by integer multiples of  $P$  chips; 2) it is not possible

to use one specific satellite's spreading code as the reference signal to remove interference for all satellites. Therefore, interference suppression must occur in a serial manner. The disadvantage is obvious as compared to the simultaneous interference removal the proposed receiver offers.

## 5.2. Interference Suppression

We next investigate the receiver's interference suppression capability by comparing it with the MMSE receiver of [16]. The MMSE receiver determines the weight vector by minimizing the mean square difference between the array output and the desired signal. The latter approach, however, requires the knowledge of the satellite direction. This condition is eliminated in the proposed scheme. If the jammers have explicit bearings, we can generate the received signals according to Equation (1.4), but replacing the spatial signature  $\mathbf{d}_k$  by the respective steering vector defined in Equation (1.6). The direction of the satellite is  $20^\circ$ , while two jammers are located at  $40^\circ$  and  $60^\circ$ . The weight vector in the MMSE method is obtained by using the exact transmitted navigation signal. Figure 6 clearly shows that deep nulls are placed at the jammer locations, whereas high gains are generated towards the direction of the satellite in both schemes. The advantage of the proposed receiver is that neither prior synchronization nor known satellite location is required.

## 5.3. Multipath Effects

The purpose of the simulations performed in this subsection is to demonstrate the difference between the receiver that solely relies on the cross-SCORE algorithm and the receiver with additional constraint in the presence of multipath. As discussed in Section 3.1, the cross-SCORE based receiver is unable to mitigate the signal multipath, though very efficient in suppressing interference, as shown by simulations presented so far. This drawback has motivated a constrained receiver design and resulted in the modified cross-SCORE algorithm based receiver in Section 3.2.

We assume that multipath reaches the receiver from the 15-degree range ( $\Omega$  as defined in Section 3.2) above the horizon. We divide  $\Omega$  into seven 2-degree spaced angles and form the corresponding matrix  $B$ . The power of the multipath component is one fifth of the direct-path signal power.

We first consider the case when there is no interference. The direct-path signal is incident on the array with  $50^\circ$  angle. One multipath component (half-chip relative delay and half the direct-path signal power) arrives from the  $9^\circ$  direction. Using the cross-SCORE based receiver, both the direct-path signal and the multipath component receive high gain at the receiver output [Figure 7(a)]. If, instead, the modified cross-SCORE based receiver is employed, the multipath contribution is significantly reduced from the output of the receiver, which is evident from Figure 7(b).

In the next case, a jammer enters into the system from  $30^\circ$ . Figure 8 shows how the two different receivers respond in this environment. We note from Figure 8(a) that both receivers can successfully place deep null at the jammer location. However, the two receivers' responses to multipath are just opposite. While the cross-SCORE based receiver generates a beam towards the multipath component, the modified cross-SCORE algorithm based receiver creates a null at the same direction.

The multipath mitigation performance of the proposed receiver is also evaluated by feeding the output of the receiver to a conventional early-late delay lock loop (DLL) [24]. We consider the discriminator functions of the receiver outputs without multipath mitigation and the outputs with the modified cross-SCORE algorithm. We compare the results with the case where there is no multipath. The early-late spacing is set to be half of the C/A chip interval. The simulation results are depicted in Figure 8(b), which clearly shows that, without any multipath mitigation process, the zero-crossing point of the discriminator function drifts away from the origin, indicating the pseudorange measurement error [30]. If, on the other hand, the modified cross-SCORE receiver is used first to mitigate multipath contributions, the zero-crossing point of the corresponding discriminator function almost overlaps with the zero-crossing point obtained using the direct-path only signal, suggesting that the proposed technique can significantly reduce the multipath effect on pseudorange measurement.

These simulations prove that both receivers have the capability of canceling strong jammers. However, for multipath mitigation, only the modified cross-SCORE algorithm based receiver can reject multipath coming from near the horizon.

#### 5.4. Synchronization Process

In satellite navigation, the receiver is ultimately evaluated by its ability to provide accurate pseudorange measurements. This is achieved by establishing synchronization between the receiver and the satellite, which is decided based on the cross-correlation between the beamformer outputs and a locally generated spreading sequence [31]. When the phase of the receiver replica code matches that of the code sequence emitted from the satellite, there is a maximum correlation. The high-gain beams towards the satellites provided in the previous examples should be examined in the context of their effects on the post-processing pseudorange calculations.

In the simulation, the satellite is located at  $20^\circ$  and the two jammers are at  $40^\circ$  and  $60^\circ$ . The figure of merit is the cross-correlation between the receiver output and the Gold code sequence:

$$C \square \frac{E\{\mathbf{z}^H \mathbf{c}\}}{\sqrt{E\{\mathbf{z}^H \mathbf{z}\} E\{\mathbf{c}^H \mathbf{c}\}}} \quad (0.37)$$

where  $\mathbf{c}$  denotes the  $P \times 1$  receiver Gold code,  $\mathbf{z}$  is a  $P \times 1$  vector with elements given by  $z(n) = \mathbf{w}^H \mathbf{x}$  and  $\mathbf{w}$  is the beamformer coefficient vector discussed in Section 3.1. The normalized cross-correlation with the respective antenna beam pattern for SNR = -25 dB and JSR = 30 dB and 50 dB are shown in Figures 9 and 10, respectively. Also shown in these figures are the normalized cross-correlations obtained before the jammers are removed. It is observed from Figure 9(b) that synchronization can be achieved in the presence of interference when JSR = 30 dB. Figure 10 shows that the proposed receiver can effectively cancel directional jammers and achieve synchronization even when the JSR is as high as 50 dB [Figure 10(c)]. Without interference suppression, however, synchronization fails as shown in Figure 10(b).

## 5.5. Circular Array

In addition to the uniform linear array, we also implemented the proposed receiver with a uniform circular array (UCA), whose configuration is shown in Figure 11(a). Let  $(\theta, \phi)$  denote the elevation angle and the azimuth angle of the satellite. Then, the steering vector of the satellite for the  $M$ -element UCA is given by

$$\mathbf{a}(\theta, \phi) = \left[ e^{j\frac{2\pi r}{\lambda} \sin \theta \cos \phi}, \dots, e^{j\frac{2\pi r}{\lambda} \sin \theta \cos \left( \phi - 2\pi \frac{M-1}{M} \right)} \right]^T \quad (0.38)$$

where  $r$  is the radius of the circular array and  $\lambda$  is the wavelength. The steering vector of the jammer has the same form as  $\mathbf{a}(\theta, \phi)$  given above. In the simulation, the satellite signal reaches the array from  $(10^\circ, 20^\circ)$ , whereas a jammer is located at  $(60^\circ, 40^\circ)$ . The beam pattern is shown in Figure 11(b) for  $r = \lambda$ , and SNR = -30 dB and JSR = 30 dB. It is observed from Figure 11(b) that the receiver has the ability to reject jammers from arbitrary directions.

## 6. Conclusions

In this chapter, we addressed the issue of interference suppression in global satellite navigation system. Specifically, the unique structure of the GNSS C/A signal is exploited. Due to the repetition of the C/A-code within each navigation symbol, strong self-coherence is observed between chip-rate sampled signals. It is shown that the use of this self-coherence feature allows the development of an anti-jamming GNSS receiving scheme which is built on the cross-SCORE algorithm. The proposed scheme incorporates multiple data and reference blocks, separated by integer multiples of the spreading code length, to generate the array weight vectors. Its performance is analyzed in view of its dependency on the number of blocks and the number of samples in each block. Two receivers are constructed based on the proposed scheme. One directly applies the cross-SCORE algorithm which seeks the optimal beamformers by maximizing the cross-correlation between the receiver output and a reference signal, derived from the receiver signal. The other one applies constraints on the beamformer such that it can also reject multipath arriving from and near the horizon. Numerical results have shown that the proposed scheme is capable of

suppressing strong wide class of narrowband and broadband interferers while preserving signals and no *a priori* knowledge of either the transmitted signals or the satellite locations is required.

## Appendix A Mean Calculation

To simplify the derivation, we rewrite the received signal vector as

$$\mathbf{x}(n) = s(n)\mathbf{a}(\theta) + \mathbf{v}(n) \quad (\text{A.1})$$

where we consider only the direct-path signal with an explicit direction  $\theta$  of the satellite. The vector  $\mathbf{v}(n)$  contains samples of interference and noise, with zero mean and variance  $\sigma_v^2$ . Both components of  $\mathbf{v}(n)$  are assumed to be independent of the GPS signal. Accordingly,

$$\mathbf{R}_s = E\{s(n)\mathbf{a}(\theta)\mathbf{a}^H(\theta)s^H(n)\} = \mathbf{a}(\theta)\mathbf{a}^H(\theta) \square \mathbf{R}_a, \quad \text{where it is assumed}$$

$$E\{s(n)s^H(n)\} = E\{|s(n)|^2\} = 1.$$

From Section 3, the estimates of the covariance matrices  $\mathbf{R}_{xx}$  and  $\mathbf{R}_{xx}^{(P)}$  are obtained using the data and reference blocks  $\mathbf{X}_N$  and  $\mathbf{X}_{Nref}$  as  $\hat{\mathbf{R}}_{xx} = \mathbf{X}_N \mathbf{X}_N^H / N$  and  $\hat{\mathbf{R}}_{xx}^{(P)} = \mathbf{X}_N \mathbf{X}_{Nref}^H / N$ , respectively. Taking the expected value  $\bar{\hat{\mathbf{R}}}_{xx}$  yields

$$\bar{\hat{\mathbf{R}}}_{xx} = E\{\hat{\mathbf{R}}_{xx}\} = \frac{1}{N} \sum_{i=0}^{N-1} E\{\mathbf{x}(n-i)\mathbf{x}^H(n-i)\} = \mathbf{R}_s + \mathbf{R}_v \quad (\text{A.2})$$

The expected value of  $\hat{\mathbf{R}}_{xx}^{(P)}$  is obtained as follows. Define the following events:

$$\begin{aligned} B_1 : & \mathbf{X}_N \text{ \& } \mathbf{X}_{Nref} \text{ are within the same symbol,} \\ B_2 : & \mathbf{X}_N \text{ or } \mathbf{X}_{Nref} \text{ is split between two adjacent symbols} \\ & \text{\& } N_1 < N \text{ samples are in the first symbol,} \\ B_3 : & \text{the entire } \mathbf{X}_N \text{ and } \mathbf{X}_{Nref} \text{ are in two adjacent symbols.} \end{aligned} \quad (\text{A.3})$$

The corresponding probabilities of the above events are:  $\Pr\{B_1\} = 1 - \frac{jP+N}{T}$ ,  $\Pr\{B_2\} = \frac{2N}{T}$ , and

$\Pr\{B_3\} = \frac{jP-N}{T}$ , respectively. In addition, we define the following events regarding the two adjacent

symbols:

$$\begin{aligned} C_1 &: \text{the two adjacent symbols have the same sign,} \\ C_2 &: \text{the two adjacent symbols have opposite signs.} \end{aligned} \quad (\text{A.4})$$

The expected value of  $\hat{\mathbf{R}}_{xx}^{(P)}$  is calculated as

$$\bar{\mathbf{R}}_{xx}^{(P)} = E\{\hat{\mathbf{R}}_{xx}^{(P)}\} = \frac{1}{N} \sum_{i=1}^N E\{\mathbf{x}(n-i)\mathbf{x}^H(n-i-jP)\} = \bar{\mathbf{R}}_{xx|B_1}^{(P)} + \bar{\mathbf{R}}_{xx|B_2}^{(P)} + \bar{\mathbf{R}}_{xx|B_3}^{(P)} \quad (\text{A.5})$$

where

$$\bar{\mathbf{R}}_{xx|B_1}^{(P)} \square \frac{1}{N} \sum_{i=1}^N E\{\mathbf{x}(n-i)\mathbf{x}^H(n-i-jP)|B_1\} \Pr\{B_1\} = \left(1 - \frac{jP+N}{T}\right) \mathbf{R}_s \quad (\text{A.6})$$

Because the GPS symbols are equi-probable, then the occurrence of  $B_3$  implies

$$\bar{\mathbf{R}}_{xx|B_3}^{(P)} \square \frac{1}{N} \sum_{i=1}^N E\{\mathbf{x}(n-i)\mathbf{x}^H(n-i-jP)|B_3\} \Pr\{B_3\} = 0 \quad (\text{A.7})$$

On the other hand, when event  $B_2$  occurs,

$$\bar{\mathbf{R}}_{xx|B_2}^{(P)} \square \frac{1}{N} \sum_{i=1}^N E\{\mathbf{x}(n-i)\mathbf{x}^H(n-i-jP)|B_2\} \Pr\{B_2\} = \frac{N}{T} \mathbf{R}_s \quad (\text{A.8})$$

From Equations (A.5 - A.8), the expected value of  $\hat{\mathbf{R}}_{xx}^{(P)}$  is given by

$$\bar{\mathbf{R}}_{xx}^{(P)} = \left(1 - \frac{jP+N}{T}\right) \mathbf{R}_s + \frac{N}{T} \mathbf{R}_s = \left(1 - \frac{jP}{T}\right) \mathbf{R}_s \quad (\text{A.9})$$

which is exactly the one shown in Equation (1.32).

When using  $G$  data and reference blocks, the estimate of the covariance matrix  $\mathbf{R}_{xx}^{(P)}$  is given by

$$\hat{\mathbf{R}}_{xxG}^{(P)} = \frac{1}{G} \sum_{g=1}^G \mathbf{X}_N(g) \mathbf{X}_{N_{\text{ref}}}^H(g) / N \quad (\text{A.10})$$

To calculate  $\overline{\hat{\mathbf{R}}}_{xxG}^{(P)}$ , the expected value of  $\hat{\mathbf{R}}_{xxG}^{(P)}$ , we define the following events:

- $F_1$ : the first data block or the last reference block is split,
- $F_2$ : one of the other  $G-1$  data/reference blocks is split  
&  $G_1 < G$  data blocks (respectively,  $G_1 - 1$  reference blocks) are in one symbol, (A.11)
- $F_3$ : the data blocks and reference blocks are within the same symbol,
- $F_4$ : no split block and the data and reference blocks are in two adjacent symbols.

The corresponding probabilities are  $\Pr\{F_1\} = \frac{N}{T}$ ,  $\Pr\{F_2\} = \frac{N}{T}$ ,  $\Pr\{F_3\} = 1 - \frac{N+GjP}{T}$ , and

$\Pr\{F_4\} = \frac{GjP - N}{T}$ . We maintain that

$$\hat{\mathbf{R}}_{xxGF_1}^{(P)} = \frac{1}{G} \sum_{g=1}^G E\{\mathbf{X}_N(g) \mathbf{X}_{N_{\text{ref}}}^H(g) | F_1\} \Pr\{F_1\} / N = \frac{N}{T} \frac{G-1}{G} \mathbf{R}_s + \frac{N}{T} \mathbf{R}_s \quad (\text{A.12})$$

and

$$\hat{\mathbf{R}}_{xxGF_2}^{(P)} = \frac{1}{G} \sum_{g=1}^G E\{\mathbf{X}_N(g) \mathbf{X}_{N_{\text{ref}}}^H(g) | F_2\} \Pr\{F_2\} / N = \frac{(G-1)N}{2T} \frac{G-2}{G} \mathbf{R}_s + \frac{(G-1)N}{2T} \mathbf{R}_s \quad (\text{A.13})$$

Further,

$$\hat{\mathbf{R}}_{xxGF_3}^{(P)} = \frac{1}{G} \sum_{g=1}^G E\{\mathbf{X}_N(g) \mathbf{X}_{N_{\text{ref}}}^H(g) | F_3\} \Pr\{F_3\} / N = \left(1 - \frac{N+GjP}{T}\right) \mathbf{R}_s \quad (\text{A.14})$$

and

$$\hat{\mathbf{R}}_{xxGF_4}^{(P)} = \frac{1}{G} \sum_{g=1}^G E\{\mathbf{X}_N(g) \mathbf{X}_{N_{\text{ref}}}^H(g) | F_4\} \Pr\{F_4\} / N = \frac{GjP - N}{2T} \frac{G-2}{G} \mathbf{R}_s + \frac{GjP - N}{2T} \mathbf{R}_s \quad (\text{A.15})$$

Finally,  $\overline{\hat{\mathbf{R}}}_{xxG}^{(P)}$  is given by

$$\overline{\hat{\mathbf{R}}}_{xxG}^{(P)} = \overline{\hat{\mathbf{R}}}_{xxGF_1}^{(P)} + \overline{\hat{\mathbf{R}}}_{xxGF_2}^{(P)} + \overline{\hat{\mathbf{R}}}_{xxGF_3}^{(P)} + \overline{\hat{\mathbf{R}}}_{xxGF_4}^{(P)} = \left(1 - \frac{jP}{T}\right) \mathbf{R}_s \quad (\text{A.16})$$

which is equivalent to the expected value given in Equation (1.32).

## Appendix B Variance Calculation

The variance of  $\hat{\mathbf{R}}_{xx}^{(P)}$  is given by [32]

$$\text{var}[\hat{\mathbf{R}}_{xx}^{(P)}] = E\{\hat{\mathbf{R}}_{xx}^{(P)}\hat{\mathbf{R}}_{xx}^{(P)H}\} - E^2\{\hat{\mathbf{R}}_{xx}^{(P)}\} \quad (\text{A.17})$$

In Appendix A, we have shown that the covariance estimates are unbiased. In what follows, we concentrate on evaluating  $E\{\hat{\mathbf{R}}_{xx}^{(P)}\hat{\mathbf{R}}_{xx}^{(P)H}\}$ .

Using one data and reference block, we let  $\Psi_{llB_l} \square E\{\hat{\mathbf{R}}_{xx}^{(P)}\hat{\mathbf{R}}_{xx}^{(P)H} | B_l\} \Pr\{B_l\}$ , where events  $B_l$ ,  $l \in [1,3]$ , are defined in Equation (A.3). Then,

$$\Psi_1 \square E\{\hat{\mathbf{R}}_{xx}^{(P)}\hat{\mathbf{R}}_{xx}^{(P)H}\} = \Psi_{llB_1} + \Psi_{llB_2} + \Psi_{llB_3} \quad (\text{A.18})$$

When the data and reference blocks are within the same symbol or, equivalently, in two adjacent symbols with the same sign (i.e., event  $C_1$ ), we have

$$E\{\hat{\mathbf{R}}_{xx}^{(P)}\hat{\mathbf{R}}_{xx}^{(P)H} | C_1\} = \frac{1}{N^2} E\left\{\sum_{i=0}^{N-1} \sum_{l=0}^{N-1} \mathbf{x}(n-i)\mathbf{x}^H(n-i-jP)\mathbf{x}(n-l-jP)\mathbf{x}^H(n-l) | C_1\right\} \quad (\text{A.19})$$

Substituting  $\mathbf{x}(n)$  from Equation (1.39) and after some straightforward calculations, we have

$$E\{\hat{\mathbf{R}}_{xx}^{(P)}\hat{\mathbf{R}}_{xx}^{(P)H} | C_1\} = \frac{M(N + \sigma_v^2)}{N} \mathbf{R}_a + \frac{M(1 + \sigma_v^2)}{N} \mathbf{R}_v \square \tilde{\mathbf{R}} \quad (\text{A.20})$$

where we have used  $\mathbf{a}^H(\theta)\mathbf{a}(\theta) = M$  and  $E\{\mathbf{v}^H(n)\mathbf{v}(n)\} = M\sigma_v^2$ . When event  $B_1$  occurs,

$$\Psi_{llB_1} = \left(1 - \frac{jP + N}{T}\right) \tilde{\mathbf{R}} \quad (\text{A.21})$$

Similarly,

$$\Psi_{1B_2} = \frac{2N}{T} \tilde{\mathbf{R}} \quad (\text{A.22})$$

and in case of event  $B_3$ , we have

$$\Psi_{1B_3} = \frac{(jP-N)}{T} \tilde{\mathbf{R}} \quad (\text{A.23})$$

Finally, the variance of  $\hat{\mathbf{R}}_{xx}^{(P)}$  is

$$\begin{aligned} \text{var}[\hat{\mathbf{R}}_{xx}^{(P)}] &= E\{\hat{\mathbf{R}}_{xx}^{(P)} \hat{\mathbf{R}}_{xx}^{(P)H}\} - E^2\{\hat{\mathbf{R}}_{xx}^{(P)}\} \\ &= \frac{M(N+\sigma_v^2)}{N} \mathbf{R}_a + \frac{M(1+\sigma_v^2)}{N} \mathbf{R}_v - \left(1 - \frac{jP}{T}\right)^2 \mathbf{R}_s^2 \end{aligned} \quad (\text{A.24})$$

For  $G$  data and reference blocks we can similarly define, using the events in Equation (A.11),

$$\Psi_G \square E\{\hat{\mathbf{R}}_{xxG}^{(P)} \hat{\mathbf{R}}_{xxG}^{(P)H}\} = \Psi_{GIF_1} + \Psi_{GIF_2} + \Psi_{GIF_3} + \Psi_{GIF_4} \quad (\text{A.25})$$

where  $\Psi_{GIF_l} \square E\{\hat{\mathbf{R}}_{xxG}^{(P)} \hat{\mathbf{R}}_{xxG}^{(P)H} | F_l\} \Pr\{F_l\}$ ,  $l \in [1,4]$ . Following the same procedure we adopted in

calculating the expected value of  $\hat{\mathbf{R}}_{xx}^{(P)}$ , it can be readily shown that

$$\begin{aligned} \Psi_{GIF_1} &= \left[ \frac{N(G-1)^2}{T G^2} + \frac{N}{T} \right] \tilde{\mathbf{R}} \\ \Psi_{GIF_2} &= \left[ \frac{(G-1)N(G-1)^2}{2T G^2} + \frac{(G-1)N}{2T} \right] \tilde{\mathbf{R}} \\ \Psi_{GIF_3} &= \left( 1 - \frac{N-GjP}{T} \right) \tilde{\mathbf{R}} \\ \Psi_{GIF_4} &= \left[ \frac{G(jP-N)(G-1)^2}{2T G^2} + \frac{G(jP-N)}{2T} \right] \tilde{\mathbf{R}} \end{aligned} \quad (\text{A.26})$$

from which we obtain

$$E\{\hat{\mathbf{R}}_{xxG}^{(P)} \hat{\mathbf{R}}_{xxG}^{(P)H}\} = \left( 1 - 2\frac{jP}{T} + 2\frac{jP}{GT} \right) \left[ \frac{M(N+\sigma_v^2)}{N} \mathbf{R}_a + \frac{M(1+\sigma_v^2)}{N} \mathbf{R}_v \right] \quad (\text{A.27})$$

Finally, the variance is

$$\begin{aligned} \text{var} \left[ \hat{\mathbf{R}}_{xx}^{(P)} \right] &= E \left\{ \hat{\mathbf{R}}_{xx}^{(P)} \hat{\mathbf{R}}_{xx}^{(P)H} \right\} - E^2 \left\{ \hat{\mathbf{R}}_{xx}^{(P)} \right\} \\ &= \left( 1 - 2 \frac{jP}{T} + 2 \frac{jP}{GT} \right) \left[ \frac{M(N + \sigma_v^2)}{N} \mathbf{R}_a + \frac{M(1 + \sigma_v^2)}{N} \mathbf{R}_v \right] - \left( 1 - \frac{jP}{T} \right)^2 \mathbf{R}_s^2 \end{aligned} \quad (\text{A.28})$$

The above equation clearly shows that the larger the number of data and reference blocks used in the time-averaging, the smaller the variance.

## References

- [1] E. D. Kaplan (eds.), *Understanding GPS: Principles and Applications*. 1em plus 0.5em minus 0.4em Artech House Publisher, 1996.
- [2] P. Enge and P. Misra, "Scanning the issue/technology," *Proceedings of The IEEE*, vol. 87, no. 1, pp. 3–15, January 1999.
- [3] J. McNeff, "The global positioning system," *IEEE Transactions on Microwave Theory and Techniques*, vol. 50, no. 3, pp. 645–652, March 2002.
- [4] R. Van Nee, "Spread spectrum code and carrier synchronization errors caused by multipath and interference," *IEEE Transactions on Aerospace and Electronic Systems*, vol. 29, no. 4, pp. 1359–1365, October 1993.
- [5] P. W. Ward, "GPS receiver interference monitoring, mitigation and analysis techniques," *Journal of the Institute of Navigation*, vol. 41, no. 4, pp. 367–391, Winter 1995.
- [6] D. Moelker, E. van der Pol, and Y. Bar-Ness, "Multiple antennas for advanced GNSS multipath mitigation and multipath direction finding," in *Proceedings of ION GPS 97*, 1997, pp. 541–550.
- [7] M. S. Braasch and A. J. V. Dierendonck, "GPS receiver architectures and measurements," *Proceedings of the IEEE*, vol. 87, no. 1, pp. 48–64, January 1999.
- [8] M. Braasch and M. DiBenedetto, "Spread spectrum ranging multipath model and validation," *IEEE Transactions on Aerospace and Electronic Systems*, vol. 37, pp. 298–303, January 2001.

- [9] P. Ward, "GPS interference and jamming issues for civil and military users," in *Short Course 323, Navtech Seminars and GPS Supply, Inc.*, Annapolis, MD, 2003, pp. –.
- [10] R. Iltis and L. Milstein, "Performance analysis of narrowband interference rejection techniques in DS spread-spectrum systems," *IEEE Transactions on Communications*, vol. 32, no. 11, pp. 1169–1177, November 1984.
- [11] L. Rusch and H. Poor, "Narrowband interference suppression in CDMA spread spectrum communications," *IEEE Transactions on Communications*, vol. 42, no. 2, pp. 1969–1979, February/March/April 1994.
- [12] L. Rusch and H. Poor, "Multiuser detection techniques for narrowband interference suppression in spread spectrum communications," *IEEE Transactions on Communications*, vol. 43, no. 2, pp. 1725–1737, February/March/April 1995.
- [13] Y. Zhang, M. G. Amin, and A. R. Lindsey, "Anti-jamming GPS receivers based on bilinear signal distributions," in *Proceedings of the 2001 Military Communications Conference (MILCOM 2001)*, vol. 2, 2001, pp. 1070–1074.
- [14] M. G. Amin and Y. Zhang, "Spatial time-frequency distributions and their applications," in *Proceedings of the 6th International Symposium on Signal Processing and its Applications*, vol. 1, 2001, pp. 254–255.
- [15] M. D. Zoltowski and A. S. Gecan, "Advanced adaptive null steering concepts for GPS," in *Proceedings of the 1995 Military Communications Conference (MILCOM 1995)*, vol. 3, 1995, pp. 1214–1218.
- [16] R. L. Fante and J. J. Vaccaro, "Wideband cancellation of interference in a GPS receive array," *IEEE Transactions on Aerospace and Electronic Systems*, vol. 36, no. 2, pp. 549–564, April 2000.
- [17] R. L. Fante and J. J. Vaccaro, "Cancellation of jammers and jammer multipath in a GPS receiver," *IEEE Aerospace and Electronic System Magazine*, vol. 13, no. 11, pp. 25–28, November 1998.

- [18] D. Moelker, E. Van Der Pol, and Y. Bar-Ness, "Adaptive antenna arrays for interference cancellation in GPS and GLONASS receivers," in *Proceedings of the IEEE 1996 Position Location and Navigation Symposium*, 1996, pp. 191–198.
- [19] Y. Zhang, M. Amin, and A. R. Lindsey, "Anti-jamming GPS receivers based on bilinear signal distributions," in *Proceedings of the MILCOM 2001*, vol. 2, 2001, pp. 1070–1074.
- [20] G. Hatke, "Adaptive array processing for wideband nulling in GPS systems," in *Proceedings of the 32nd Asilomar Conference on Signals, Systems and Computers*, vol. 2, 1998, pp. 1332–1336.
- [21] P. Xiong, M. J. Medley, and S. N. Batalama, "Spatial and temporal processing for global navigation satellite systems: The GPS receiver paradigm," *IEEE Transactions on Aerospace and Electronic Systems*, vol. 39, no. 4, pp. 1471–1484, October 2003.
- [22] B. Townsend and P. Fenton, "A practical approach to the reduction of pseudorange multipath errors in a L1 GPS receiver," in *Proceedings of the 1994 ION GPS Conference*, 1994, pp. 20–23.
- [23] B. Townsend and P. Fenton, "Performance evaluation of the multipath estimating delay lock loop," in *Proceedings of the 1995 ION National Technical Meeting*, 1995.
- [24] A. Van Dierendonck, P. Fenton, and T. Ford, "Theory and performance of narrow correlator spacing in a GPS receiver," *Journal of The Institute of Navigation*, vol. 39, no. 2, pp. 265–283, 1992.
- [25] R. J. Van Nee, "The multipath estimation delay lock loop: Approaching theoretical limits," in *Proceedings of the 2nd IEEE Symposium on Spread Spectrum Techniques and Applications*, 1992, pp. 39–42.
- [26] P. Misra and P. Enge, *Global Positioning System, signals, Measurements, and performance*. Lincoln, Massachusetts: Ganga-Jamuna Press, 2001.
- [27] B. Agee, S. Schell, and W. Gardner, "Spectral self-coherence restoral: A new approach to blind adaptive signal extraction using antenna array," *Proceedings of the IEEE*, vol. 78, no. 4, pp. 753–767, April 1990.

- [28] B. Agee, S. Schell, and W. Gardner, "The score approach to blind adaptive signal extraction: An application of the theory of spectral correlation," in *Proceedings of the Fourth Annual ASSP Workshop on Spectrum Estimation and Modeling*, 1988, pp. 277–282.
- [29] G. H. Golub and C. F. Van Loan, *Matrix Computations*, 3rd ed. Baltimore, MD: Johns Hopkins University Press, 1996.
- [30] M. S. Braasch and A. J. V. Dierendonck, "GPS receiver architectures and measurements," *Proceedings of the IEEE*, vol. 87, no. 1, pp. 48–64, January 1999.
- [31] B. W. Parkinson and J. J. Spilker Jr. (eds.), *Global positioning system: Theory and applications, Vol I*. American Institute of Aeronautics, Inc., Washington, DC: Progress in Astronautics and Aeronautics, 1996.
- [32] A. Papoulis, *Probability, Random Variables, and Stochastic Processes*, 3rd ed. McGraw-Hill, 1991.

# Figures

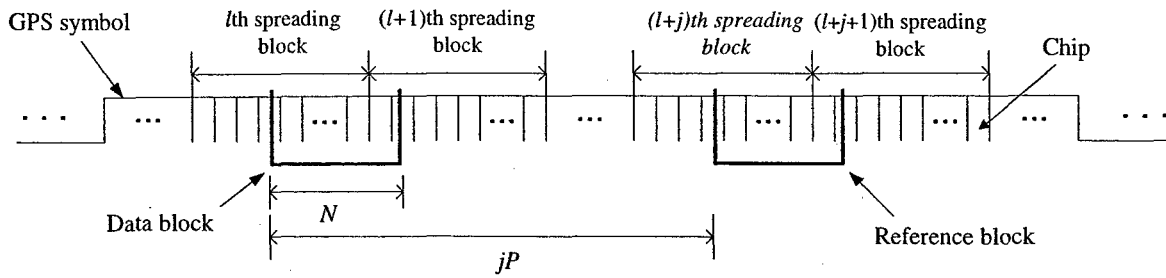


Figure 1. Noise-free C/A signal structure and data and reference blocks formation.

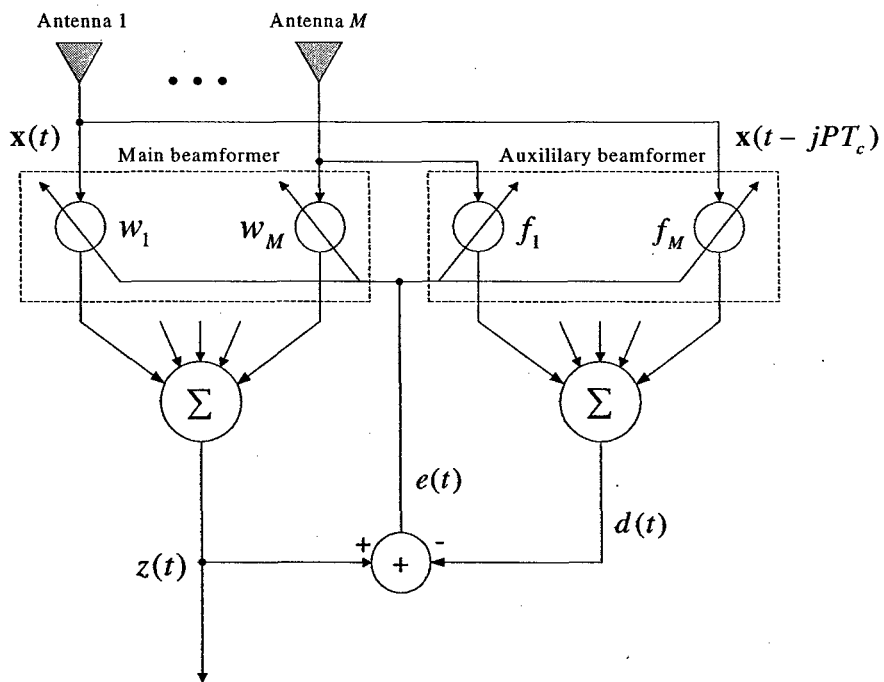


Figure 2. Structure of the proposed anti-jamming scheme.

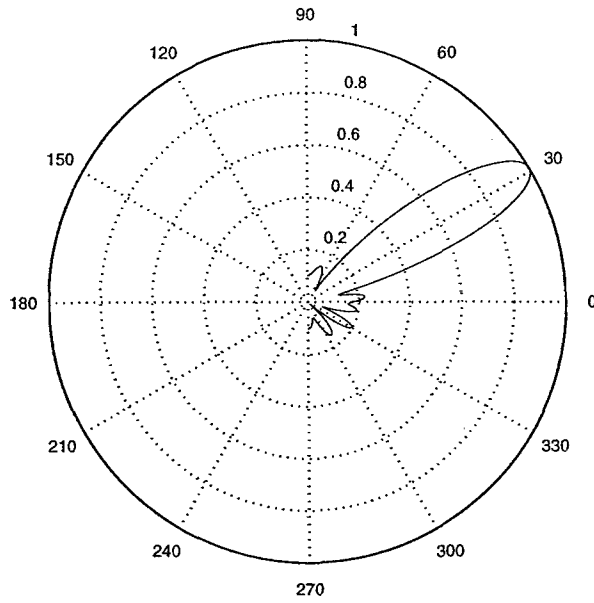


Figure 3. Beam pattern generated by the cross-SCORE based receiver with  $\text{SNR} = -30$  dB and one data and one reference block taking within the same symbol.

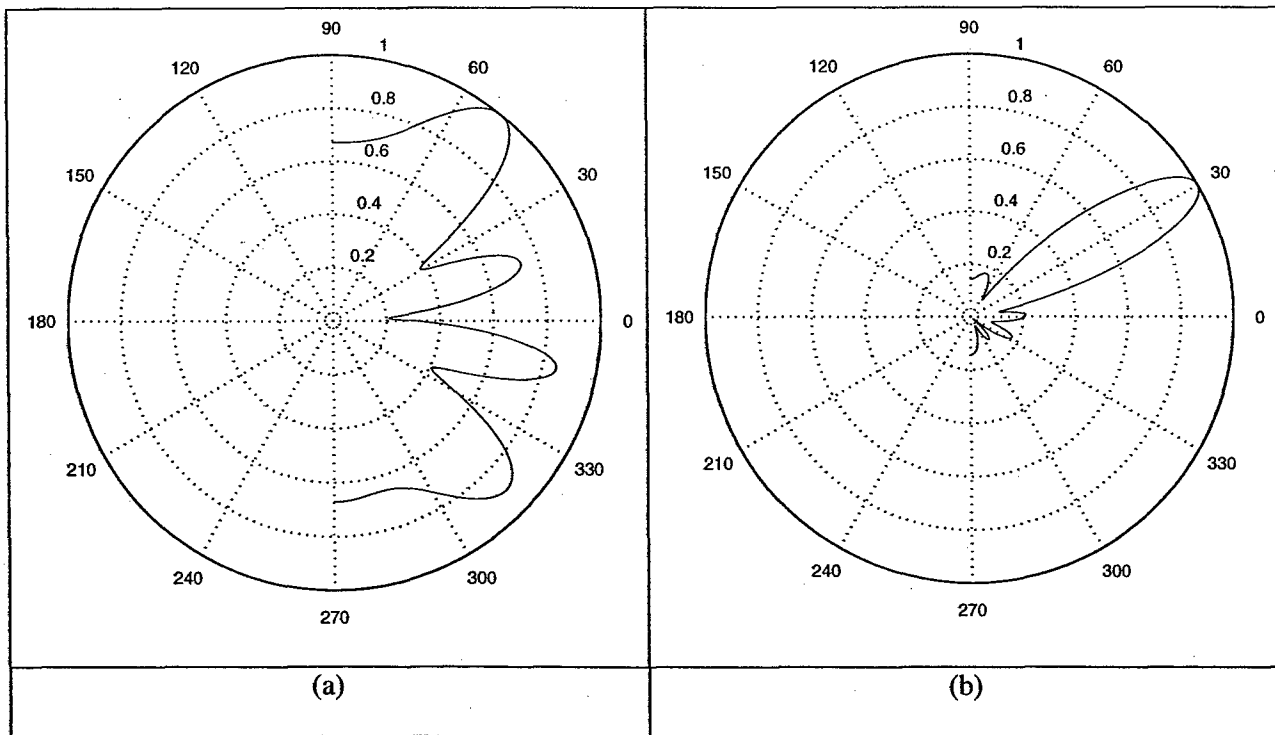


Figure 4. Beam pattern generated by the cross-SCORE based receiver with multiple data and reference blocks and  $\text{SNR} = -40$  dB. (a)  $G = 2$ ; (b)  $G = 7$ .

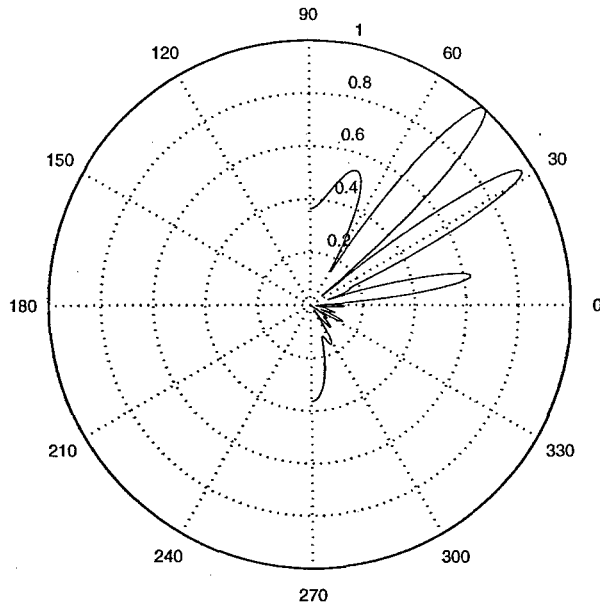


Figure 5. Beam pattern generated by the cross-SCORE based receiver with four satellites, SNR = -30 dB, and  $G = 7$ .

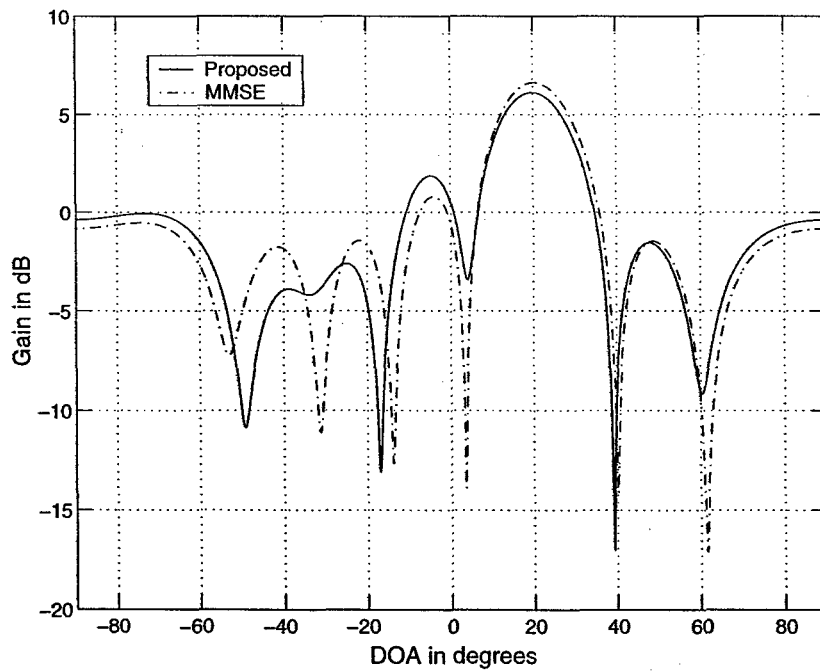


Figure 6. Antenna gains of the proposed scheme and the MMSE scheme with SINR = -33 dB, JSR = 30 dB, and  $G = 3$ .

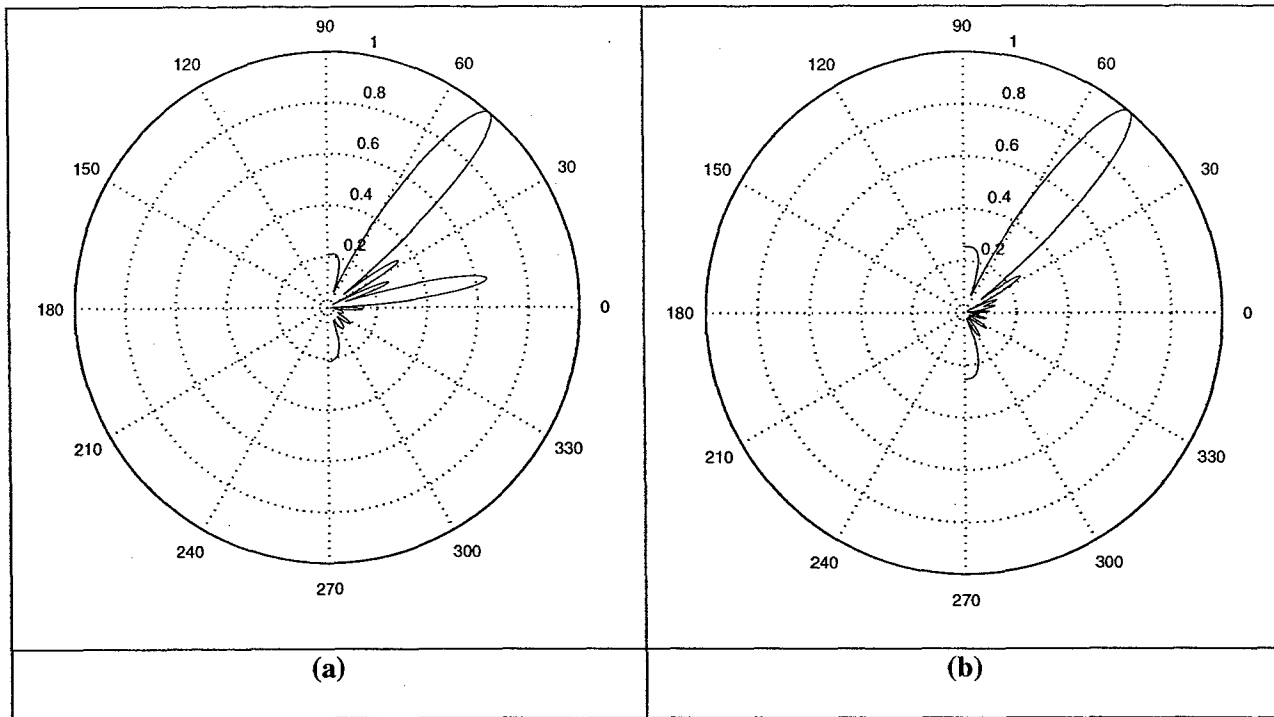


Figure 7. In the presence of multipath with  $SNR = -30$  dB and  $G = 7$ . (a) Cross-SCORE based receiver; (b) Modified cross-SCORE based receiver.

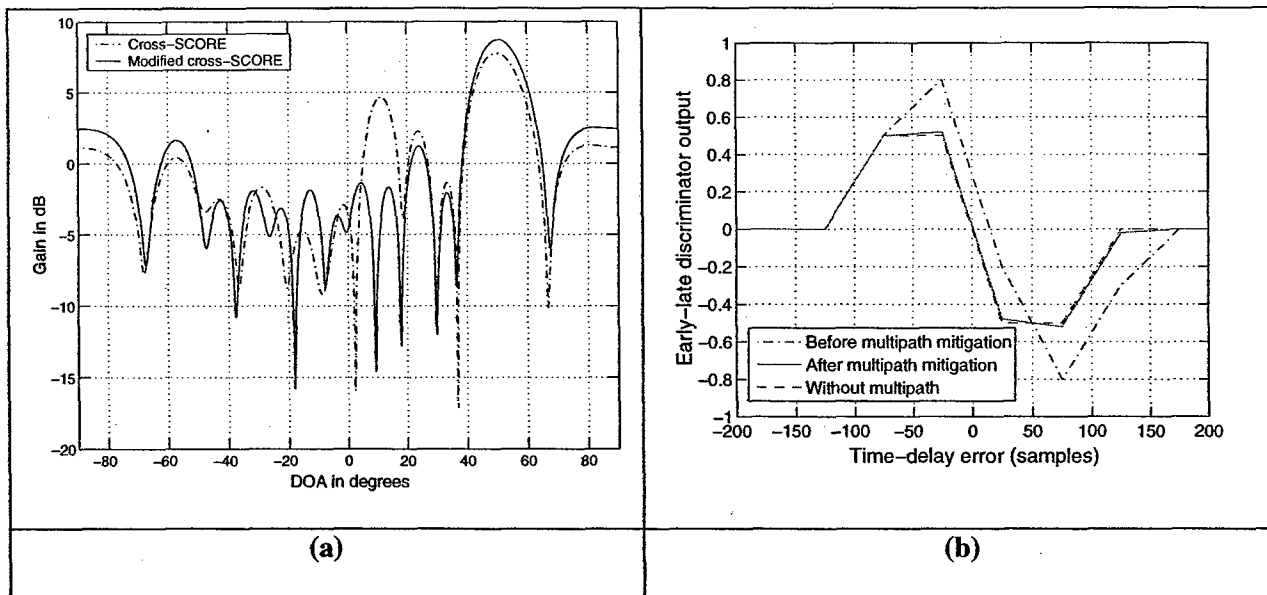
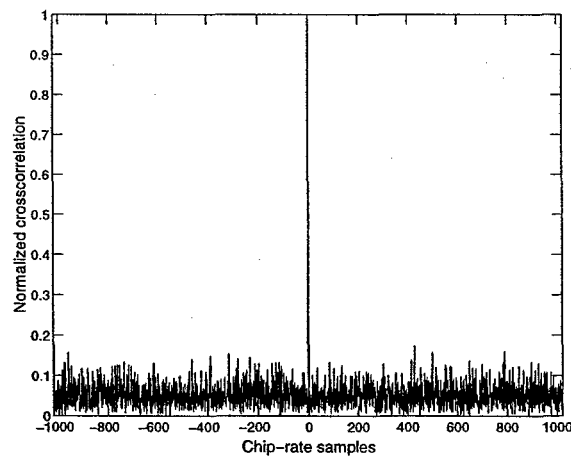
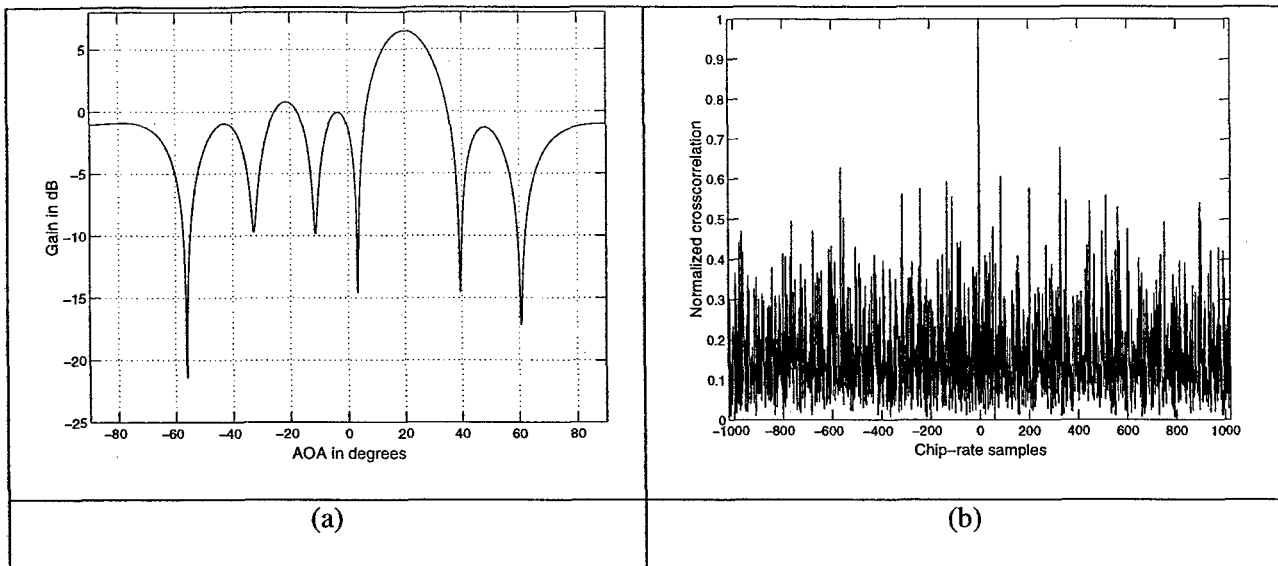


Figure 8. (a) Comparison between the cross-SCORE based receiver and the modified cross-SCORE based receiver  $SINR = -33$  dB,  $JSR = 30$  dB, and  $G = 7$ ; (b) Comparison of the discriminator functions of the early-late delay lock loop.



(c)

Figure 9. Synchronization of the cross-SCORE based receiver with  $\text{SNR} = -25$  dB,  $\text{JSR} = 30$  dB, and  $G = 7$ . (a) Beam pattern; (b) Normalized cross-correlation before jammer removal; (c) Normalized cross-correlation after jammer removal.

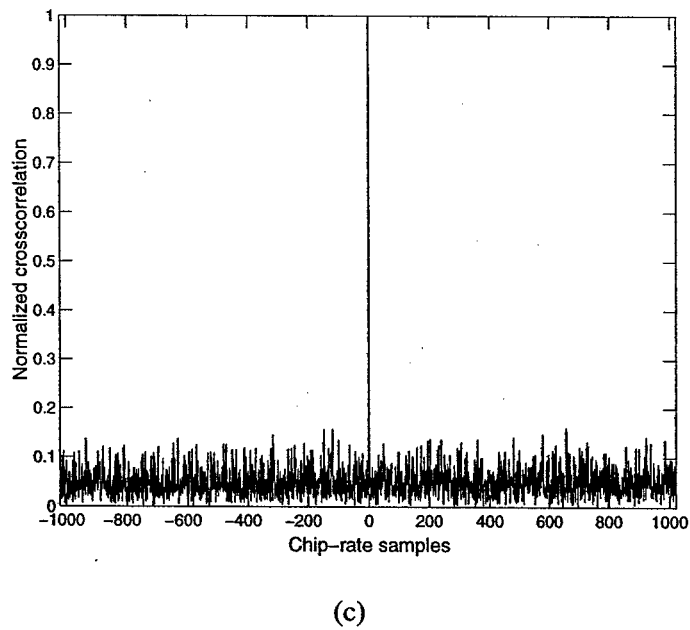
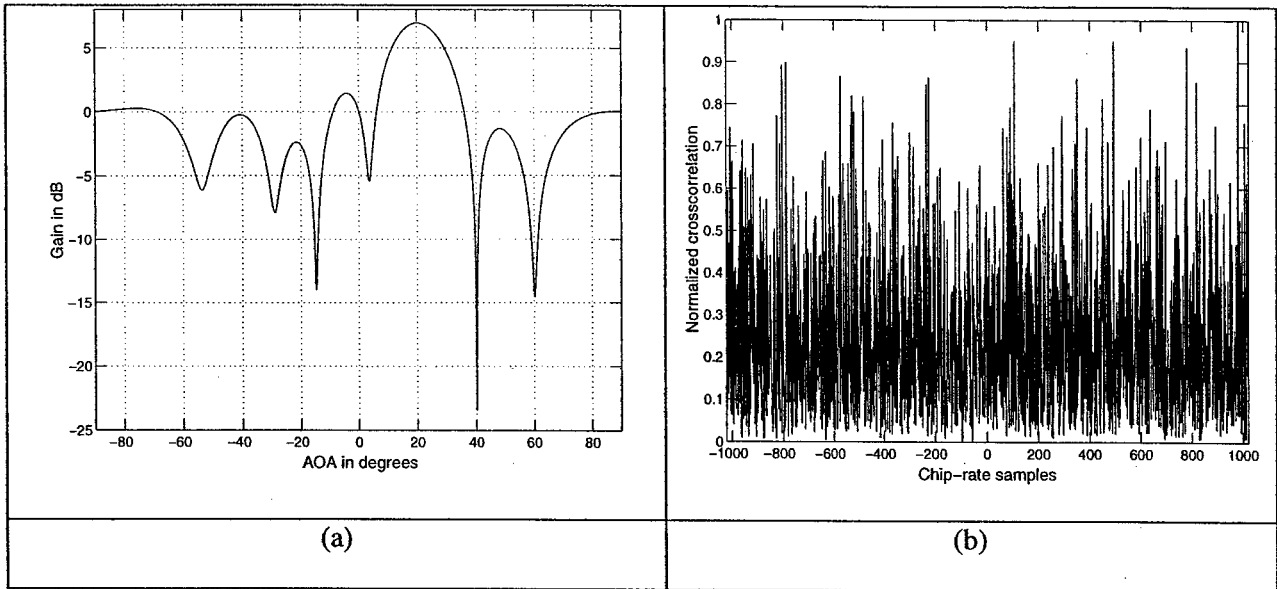


Figure 10. Synchronization of the cross-SCORE based receiver with  $\text{SNR} = -25$  dB,  $\text{JSR} = 50$  dB, and  $G = 7$ . (a) Beam pattern; (b) Normalized cross-correlation before jammer removal; (c) Normalized cross-correlation after jammer removal.

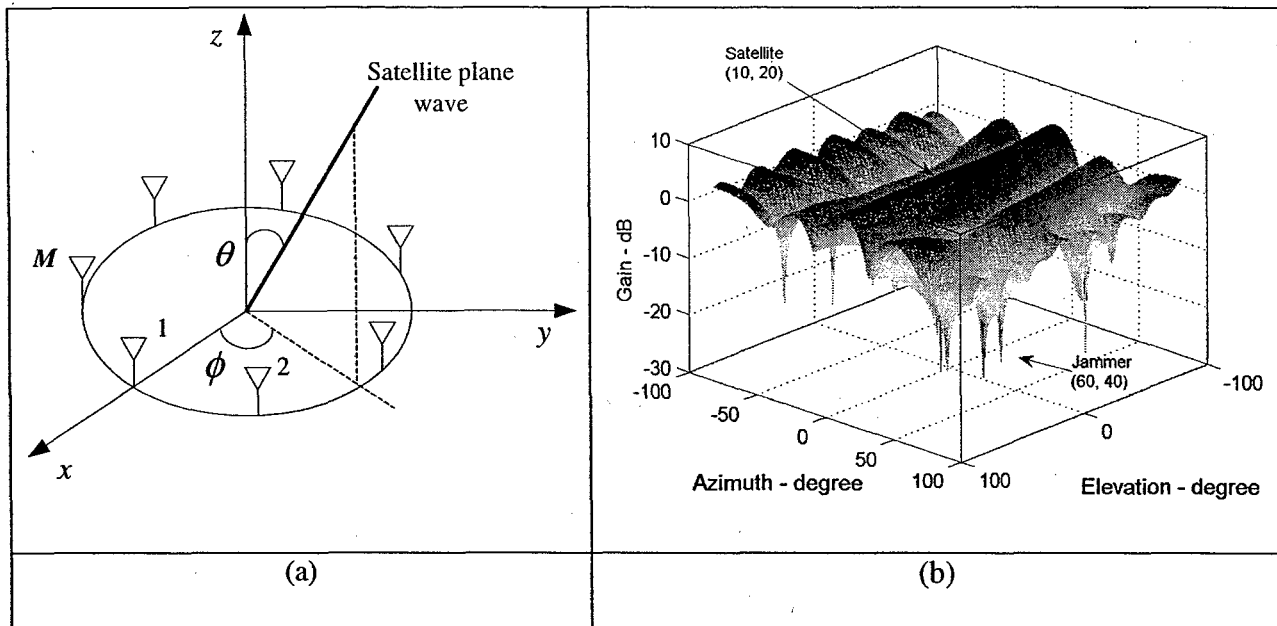


Figure 11. Performance of the receiver with a circular array. (a) Circular array configuration; (b) Beam pattern.

## Chapter 2

# Performance Analysis of GPS Receivers in Non-Gaussian Noise Incorporating Precorrelation Filtering and Sampling Rate

### 1. Introduction

The GPS receiver is subject to noise and jamming, in addition to multipaths. The effect of multipath on the GPS receiver performance has been extensively analyzed [1-5], whereas several anti-jam GPS techniques have been proposed for suppressing narrowband, wideband, noise-like and chirp-like jammers [6-8]. This chapter focuses on effect of various noise sources on GPS receiver performance.

With the growing needs for indoor GPS and demands of the satellite-based navigation in manned and autonomous ground, aerial, and surface vehicles, the GPS receivers are required to operate in close proximity to various noise sources of Gaussian and non-Gaussian characteristics. These sources compromise the receiver performance by impeding signal acquisition and increasing the bit error rates [9]. Sources of non-Gaussian noise may include motor ignition noise, which is generated by spark plugs used in internal combustion engines [10], impulsive and noise radars for imaging [11], and ultra-wideband (UWB) emitters [12,13]. The latter is becoming the choice of signals in imaging and wideband communication platforms [14-18]. The UWB sources and noise radar have bandwidths that can extend over HF, VHF, UHF, and beyond, including the GPS band. The transmission of repeated short pulses in UWB systems contributes to their possible impulsiveness nature. Noise radars [11], are seeing increased applications in indoor and outdoor target detection and tracking. Although the pulse amplitude and intervals of transmission are fixed, multipath returns bring randomness to non-intended receivers, including GPS. On the other hand, the frequency range of motor ignition noise is approximately 100 MHz ~ 10 GHz [19,20], which overlaps with the GPS band.

One of the main contributions of this chapter is to show the effect of non-Gaussian noise on the GPS receiver performance, specifically, its delay lock loop (DLL). We consider impulsive noise, described by three different canonical models, namely, Middleton noise [21], generalized Cauchy noise [22] and symmetric  $\alpha$ -stable (S $\alpha$ S) noise [23]. We also examine the automotive ignition noise and UWB noise models based on the empirical data provided in [24,25].

It is well known that DLL is the main component of the GPS receiver which performs acquisition and provides the pseudo ranging. The DLL correlates the incoming digital intermediate frequency (IF) signal with the C/A reference code from three different shifting positions, referred to as early, late and punctual. The results are then sent into a discriminator for arithmetic processing. Commonly, the system asserts the synchronization when the discriminator output is null. However, the correlator noise components, which result from the correlation between the incoming noise sources and the early, late and punctual C/A reference codes, lead to a tracking error and loss of accurate synchronization. In this chapter, we evaluate the impact of the non-Gaussian noise on the DLL discriminator performance, incorporating the effect of the front-end bandpass precorrelation filter and sampling rate. The precorrelation filter reduces the out-of-band noise and interference, but also increases the correlation between noise samples, which in turn, increases the discriminator tracking error. Both the tracking error variance and the discriminator error variance are derived and shown to be highly dependent on the signal-to-noise ratio (SNR), sampling rate, and precorrelation filter bandwidth. We utilize the fact that due to the long time-averaging typically performed in GPS receivers using a large number of C/A chips, the central limit theorem (CLT) can be applied to characterize the correlator output noise components, which are shown to be Gaussian.

Section 2 provides an overview of commonly used and known non-Gaussian noise models. The precorrelation filter and its effect on the DLL discriminator performance are discussed in Section 3. Requirements on the filter bandwidth and sampling rate are also established. The expressions of discriminator errors and their statistical characteristics in noise are derived in Section 4 in terms of

sampling rate and precorrelation filter bandwidth. Computer simulations are provided in Section 5 and compared with the theoretical results.

## 2. Non-Gaussian Noise Models

In this section, we briefly discuss several commonly used non-Gaussian noise models. We present the noise probability density function (PDF) and show corresponding sample realization. These noise sources are employed in the GPS receiver analysis and simulations throughout the section.

### A. SaS Noise Model

The  $\alpha$ -stable model [23,26], which exhibits sharp spikes and occasional bursts, is typically used for describing the impulsive phenomena. The standard SaS PDF is given by

$$f(z) = \frac{1}{\pi} \sum_{k=1}^{\infty} \frac{(-1)^{k-1}}{k!} \Gamma(\alpha k + 1) |z|^{-\alpha k - 1} \sin\left[\frac{k\alpha\pi}{2}\right], \quad 0 < \alpha < 1 \quad (1)$$

$$f(z) = \frac{1}{\pi\alpha} \sum_{k=0}^{\infty} \frac{(-1)^k}{2k!} \Gamma\left(\frac{2k+1}{\alpha}\right) z^{2k}, \quad 1 < \alpha < 2 \quad (2)$$

The parameter  $\alpha$  assumes values in the range (0, 2] and measures the “thickness” of the tails of the distribution. A small value of  $\alpha$  implies considerable probability mass in the tails of the distribution, which means “severe impulsive”. There are two important special cases; the PDF is Gaussian for  $\alpha = 2$ , and Cauchy for  $\alpha = 1$ . Figure 1(a) shows the PDF of SaS noise, whereas Figure 1(b) presents a sample noise sequence for  $\alpha = 0.5$ .

### B. Middleton Noise Model

Middleton impulsive noise model [21] is composed of both Gaussian and impulsive noise components. The probability density function (PDF) is defined by two parameters  $A$  and  $\Gamma$ . The term  $A$  represents the product of the average duration of the pulse and the average number of pulses occurring in unit time. Small values of  $A$  increase the impulsiveness of the noise, whereas large values of  $A$  move the model closer to a Gaussian distribution. The parameter,  $\Gamma = \sigma_G^2 / \sigma_I^2$ , is defined as the Gaussian-to-impulsive

noise power ratio, where  $\sigma_G^2$  represents the Gaussian noise power and  $\sigma_I^2$  is the impulsive noise power.

The total noise power is

$$\sigma^2 = \sigma_G^2 + \sigma_I^2 \quad (3)$$

and the PDF is given by

$$p(z) = \sum_{m=0}^{\infty} \frac{e^{-A} A^m}{m!} \cdot \frac{1}{\sqrt{2\pi\sigma_m^2}} \exp\left(-\frac{|z|^2}{2\sigma_m^2}\right) \quad (4)$$

with

$$\sigma_m^2 = \frac{(m/A) + \Gamma}{1 + \Gamma} \quad (5)$$

If  $A$  is sufficiently small, then the model can be simplified by only retaining the dominant terms in (4) corresponding to  $m = 0, 1, 2$  [27]. In this case, the noise PDF function, shown in Figure 2(a), can be approximated by

$$p_z(z) = \sum_{m=0}^2 \frac{e^{-A} A^m}{m!} \cdot \frac{1}{\sqrt{2\pi\sigma_m^2}} \exp\left(-\frac{|z|^2}{2\sigma_m^2}\right) \quad (6)$$

The above PDF is an even function with heavy tails, as illustrated in Figure 2(a). A sample of Middleton noise sequence is depicted in Figure 2(b).

### C. Generalized Cauchy Noise Model

A generalized Cauchy probability density function [22] is defined in terms of three parameters,  $\sigma^2$ ,  $k > 0$  and  $\nu > 0$ ,

$$p(z) = \frac{B}{\left\{1 + \frac{1}{\nu} \left[\frac{|z|}{A}\right]^k\right\}^{\nu+1/k}} \quad (7)$$

where

$$A = \left[\sigma^2 \frac{\Gamma(1/k)}{\Gamma(3/k)}\right]^{1/2}, \quad B = \frac{k\nu^{-1/k}\Gamma(\nu+1/k)}{2A\Gamma(\nu)\Gamma(1/k)} \quad (8)$$

In the above equations,  $\Gamma(\cdot)$  is the Gamma function, given by

$$\Gamma(a) = \int_0^{\infty} x^{a-1} e^{-x} dx \quad (9)$$

The parameter  $k$  controls the impulsiveness of the noise, whereas  $v$  defines the noise variance and  $\sigma^2$  is a scale parameter. In the example shown in Figure 3(a), we set  $k = 0.2$ ,  $v = 40$ , and  $\sigma^2 = 4.7$ . Figure 3(b) shows the sample sequence of the noise.

#### D. Ignition Noise Model

The motor ignition noise model deduced from experiment data [24] is a statistical process consisting of two distributions: a Weibull distribution, due to the high power peaks, and a Gaussian distribution, due to low power values. These distributions are shown in Figure 4(a) and 4(b), respectively. The Weibull distribution PDF is given by

$$p(z) = ab^{-a} z^{a-1} e^{-(z/b)^a} \quad (10)$$

We set  $a = 1.14$  and  $b = 4.00$  in Figure 4(a). The inter-arrival times between successive noise peaks are shown to be exponentially distributed, as illustrated in Figure 4(c). A sample noise sequence is shown in Figure 4(d). The middle strip in the figure corresponds to Gaussian distribution and the spikes are weibull distributed.

#### E. UWB Noise Model

The UWB signal has been widely surveyed. The signal can be cast as impulsive noise since it consists of intermittent pulses [28-30]. The statistics of UWB type of noise generated using multiple UWB signal sources are reported in [25] based on several data measurements. With the assumption that the phases of the band-limited UWB signals are uniformly distributed, it was concluded that the amplitude of the aggregate UWB signals approximates a Rayleigh distribution, which is shown in Figure 5(a). Figure 5(b) gives the sample sequence of the noise with unit variance.

#### F. Noise Radar Waveform Model

An ultra-wideband radar is a radar whose fractional bandwidth relative to the carrier or the center frequency is greater than 0.25. It transmits ultra-wideband noise or noise-like waveform towards the

target [12]. The advantage of this technique lies in the relative immunity of the random noise-like unpolarized transmit signal from detection and jamming. The random noise is modeled as

$$N(t) = A(t) \cos[2\pi(f + \Delta f)t] \quad (11)$$

Typically,  $A(t)$  is Rayleigh distributed and  $\Delta f$  is uniformly distributed between  $[-0.5\text{GHz}, +0.5\text{GHz}]$ . The center frequency of the noise waveform is set to 1.5 GHz [12]. It is assumed that  $A(t)$  and  $\Delta f$  are uncorrelated random processes. The amplitude PDF of the noise is shown in Figure 6(a), and a sample realization is shown in Figure 6(b).

### 3. Sampling and Filtering Effects

In this section, we discuss the effects of sampling rate and filter bandwidth on the GPS receiver. Conditions on both variables for proper tracking and synchronization are established.

The main operation for code synchronization in the DLL is the cross-correlations performed between the received data and the receiver reference code. Figure 7 shows three pairs of correlators required to produce three in-phase components,  $I_E$ ,  $I_P$ ,  $I_L$  and three quadrature components  $Q_E$ ,  $Q_P$ ,  $Q_L$ , respectively, corresponding to the early (E), punctual (P) and late (L) reference C/A codes. These codes are generated from three shifting code positions, but with the same intervals. By processing the above six components, the receiver may construct at least three different DLL discriminators [31], namely,

*Coherent*

$$D = (I_E - I_L) \text{sign}(I_P) \quad (12)$$

*Early-minus-late power (noncoherent)*

$$D = (I_E^2 + Q_E^2) - (I_L^2 + Q_L^2) \quad (13)$$

*Dot-product (noncoherent)*

$$D = (I_E - I_L)I_P + (Q_E - Q_L)Q_P \quad (14)$$

where  $\text{sign}(I_p)$  is the sign of the navigation message data bit. Synchronization is reached by locating the correlation peak. Commonly, the discriminator determines the peak correlation location by reaching zero output value. The output of correlator  $j$  ( $j = E, P, L$ ), corresponding to the early, punctual, or late shifting positions, can be written as [32].

$$I_j = \sqrt{2STR(\tau_j)} \cos \varphi + \eta_{Ij}, \quad Q_j = \sqrt{2STR(\tau_j)} \sin \varphi + \eta_{Qj} \quad (15)$$

where  $S$  is the signal power,  $\varphi$  is the residual phase error,  $R(\tau_j)$  is the cross-correlation function between the incoming C/A code and the reference code corresponding to a delay  $\tau_j$  and performed over  $T$  (usually 0.001) seconds. In the above equation,  $\eta_{Ij}$  and  $\eta_{Qj}$  are the in-phase and quadrature noise components of the correlator outputs. Clearly, if  $g_{j,\ell}$  are the reference code sample sequence, and  $n_{Ij,\ell}$  and  $n_{Qj,\ell}$  represent the input noise samples, then the in-phase and quadrature noise components can be expressed as

$$\eta_{Ij} = \sum_{\ell=1}^M g_{j,\ell} n_{Ij,\ell}, \quad \eta_{Qj} = \sum_{\ell=1}^M g_{j,\ell} n_{Qj,\ell} \quad (16)$$

where  $M = K_0 T$  is the number of samples employed in the computation of the cross-correlation (usually it is an integer multiple of 1023), and  $K_0$  is the sampling rate.

#### A. Sampling Rate

The C/A code consists of 1023 chips. In order to generate the proper early-late correlation functions for the discriminator, the required number of samples per chip,  $K$ , becomes dependent on the early-late correlator spacing  $d$ . The synchronization position typically exists at the midpoint between the two peaks of the early and late correlation functions. Therefore, in order to accurately find the synchronization point, at least 2 samples should be generated over the linear range of the early-late correlator spacing. This requires, at minimum, one sample for each half correlator spacing,  $\frac{d}{2}$ . If we express the spacing as

$d = \frac{m}{n}$  fraction of a chip, where  $m$  and  $n$  are both integers, forming an irreducible fraction, then half

spacing is  $\frac{m}{2n}$ . Therefore, the integer number of samples per chip,  $K$ , should be no less than  $2n$ , if  $m$  is

not a multiple of 2, while  $K$  should be no less than  $n$ , if  $m$  is a multiple of 2. For instance, if the early-late correlator spacing is  $3/5$  chips, then the number of samples per chip should be at least 10, where as if  $d = 2/5$  chips, then  $m = 2$ , and  $K$  should be at least equal to 5. Details of this example are shown in Figure 8(a), wherein the early-late correlator functions with spacing of  $2/5$  chips can be implemented by the sampling rate of 5 samples per chip. The discriminator function shown in Figure 8(b) describes the discriminator output due to the tracking error. It is the difference between the early-late correlation functions. Without multipath and noise, the discriminator output, assumes zero value at synchronization, which can be estimated by two reference points and by utilizing the linearity over the delay error range of the discriminator function. In Figure 9 (a) and (b), we reduce the sampling rate to 3 samples per chip. It is evident that in this case, we could not estimate the correct synchronization point, since the sampling rate doesn't provide sufficient resolution for holding the two reference points in the linear range.

### B. Precorrelation Filtering

A precorrelation filter is applied to filter out noise and interference outside the GPS bandwidth. Code tracking accuracy in white noise has been examined for an infinite precorrelation bandwidth [31]. Filters with finite bandwidth cause correlation changes of the received signals and remove the sidelobes of C/A code spectrum. Figure 10 shows the GPS frequency spectrum due to the application of a Butterworth filter of 2 MHz bandwidth. Typically, the filtering adds a delay to the incoming C/A code relative to the local C/A code. The direct result is the offset of the peak location of the correlation function. Figure 11 shows the cross-correlation function between the filtered C/A code and the local original C/A code. It is observed that the function's peak location does not correspond to zero time delay error, yielding a tracking error. In order to compensate for the delay, one solution is to subtract the known induced filter delay from the overall delay. However, even with delay correction, and as evident from Figure 11, the correlation function due to filtering is not absolutely symmetric. This leads to a slight deflection of zero-delay error point in the discriminator function, which is shown in Figure 12. For accuracy, the induced deflection should also be corrected.

One way to mitigate the filter effect is to apply the same precorrelation filter to the local C/A code. The correlators of DLL would now process the incoming and local filtered C/A codes. Figure 13 shows the C/A code autocorrelation function after applying the precorrelation filtering using different values of the filter bandwidth. The autocorrelation function is symmetric with no delay bias. It is clear from Figure 13 that the autocorrelation function changes, depicting a more smoothed shape for narrower filter bandwidth, and as much, compromising the linear range of the discriminator.

#### 4. GPS DLL Performance under Different Noise Sources

The precorrelation filter also modifies the correlation properties of the noise, when added to the received signal. The ideal band-limited filtered noise has a sinc autocorrelation function, which in baseband, is given by

$$R_{fn}(\tau) = \frac{\sin(\pi B_f \tau)}{\pi B_f \tau} \quad (17)$$

where  $B_f$  is the precorrelation filter bandwidth. In Figure 14, for  $B_f = 1$  MHz, the noise samples spaced equal to or larger than 1 microsecond (the chip width) are either uncorrelated or weakly correlated. In essence, oversampling causes the sampling interval to be smaller than the chip width, yielding correlated noise samples. The latter adversely affects the discriminator performance and forces the discriminator output to assume zero values at the wrong signal propagation delay, i.e., incorrect satellite range. Figure 15 shows an example of the distorted correlation functions and corresponding discriminator function of the C/A code with additive filtered generalized Cauchy noise with  $\text{SNR} = -10$  dB.

In order to evaluate the discriminator performance in noise, the variance expressions for different noise components of the correlator outputs should be derived. A data sample in the noise sequence can be considered as a random variable. After passing through the precorrelation filter, the noise samples change both their distributions and correlation functions, depending on the filter bandwidth. For instance, Figure 16 shows the PDF and the sample sequence of the filtered Middleton noise. Compared with the original PDF of Figure 2, it is clear that the impulsiveness and density have been reduced due to filtering.

However, the uncorrelated noise samples, whose spacing is equal to the half of the main lobe of the autocorrelation function, are still i.i.d. (independent, identical distribution).

To derive the noise error variance at the filter output, we group the noise samples into several sequences, each includes uncorrelated noise samples separated by an inverse of the filter bandwidth. The correlator output, therefore, is the sum of the correlations between the receiver reference C/A code and the different grouped noise sequences. It is noted that due to long time averaging imposed by the correlation loop, the Central Limit Theorem (CLT) can be applied, yielding a Gaussian random distribution for the output of each noise sequence. As a result, for the sampling rate of  $K$  samples per chip, the above correlation process yields  $K$  Gaussian random variables, the sum of which is also Gaussian. Accordingly, the in-phase and quadrature noise components,  $\eta_{ij}$  and  $\eta_{Qj}$ , in (16) are both Gaussian. The histograms of those two components for the case of filtered Middleton noise using 2 samples per chip are shown in Figure 17. The Gaussian shape is evident.

We consider the early-minus-late power discriminator. From (13) and (15), the discriminator output is

$$\begin{aligned} D &= (I_E^2 + Q_E^2) - (I_L^2 + Q_L^2) \\ &= (\sqrt{2STR}(\tau_E) \cos \varphi + \eta_{IE})^2 + (\sqrt{2STR}(\tau_E) \sin \varphi + \eta_{QE})^2 \\ &\quad - (\sqrt{2STR}(\tau_L) \cos \varphi + \eta_{IL})^2 - (\sqrt{2STR}(\tau_L) \sin \varphi + \eta_{QL})^2 \end{aligned} \quad (17)$$

where

$$\tau_E = \tau_p + d/2, \quad \tau_L = \tau_p - d/2 \quad (18)$$

and

$$R(\tau_E) = R(\tau_p + d/2) = 1 - (\tau_p + d/2), \quad R(\tau_L) = R(\tau_p - d/2) = 1 + (\tau_p - d/2) \quad (19)$$

assuming the prompt time delay  $\tau_p$  is bounded into the discriminator linear working range. When  $D = 0$ , the tracking error  $\rho$  can be expressed as

$$\rho = \tau_p \Big|_{D=0} = \frac{\eta_{IE}^2 + \eta_{QE}^2 - \eta_{IL}^2 - \eta_{QL}^2 + 2\sqrt{2ST}(1-d/2)[(\eta_{IE} - \eta_{IL}) \cos \varphi + (\eta_{QE} - \eta_{QL}) \sin \varphi]}{8ST(1-d/2)} \quad (20)$$

The variance of the tracking error

$$\text{Var}(\rho) = \frac{(E[\eta_{IE}^2])^2 - (E[\eta_{IE}\eta_{IL}])^2 + 2ST(1-d/2)^2(E[\eta_{IE}^2] - E[\eta_{IE}\eta_{IL}])}{8S^2T^2(1-d/2)^2} \quad (21)$$

where  $E[*]$  is the statistical expectation operation. In the above equation,

$$E[\eta_{IE}^2] = P_n [M + 2 \sum_{i=1}^{K-1} (M-i)R_f(i)R_{fn}(i)] \quad (22)$$

$$E[\eta_{IE}\eta_{IL}] = P_n \left\{ (1-d)M + \sum_{i=1}^{K-Kd-1} (M-i)R_f(i+Kd)R_{fn}(i) + \sum_{i=1}^{K+Kd-1} (M-i)R_f(|Kd-i|)R_{fn}(i) \right\} \quad (23)$$

where  $P_n$  is the normalized filtered noise variance,

$$P_n = \frac{N_0 B_f T}{M} \quad (24)$$

in which  $N_0$  is the noise spectral density. In equation (22) and (23), we used the autocorrelation function of the C/A code,

$$R_f(i) = 1 - i/K \quad \text{for } i = 1, 2, \dots, K-1; \quad R_f(i) = 0 \quad \text{for } i = K, K+1, \dots, M \quad (25)$$

and the noise autocorrelation function,

$$R_{fn}(i) = \frac{\sin(i\pi B_f / B_s)}{i\pi B_f / B_s} \quad \text{for } i = 1, 2, \dots, M \quad (26)$$

As a reminder,  $K$  is the number of samples per chip,  $M$  is the total number of samples,  $B_f$  is the precorrelation filter bandwidth, and  $B_s$  is the sampling frequency. Typically,

$$M = 1023K, \quad B_s = K \times 10^6 \quad (27)$$

The derivation of the above equations is given in APPENDIX A.

All terms in (21) are highly dependent on SNR, defined as  $(\text{SNR} = 10 \log_{10}(S/N_0 B_f))$ . For relatively high SNR, the term  $(E[\eta_{IE}^2])^2 - (E[\eta_{IE}\eta_{IL}])^2$  is relatively small, compared with  $2ST(1-d/2)^2(E[\eta_{IE}^2] - E[\eta_{IE}\eta_{IL}])$ . Thus, (21) can be simplified to

$$\text{Var}(\rho) \approx \frac{2ST(1-d/2)^2(E[\eta_{IE}^2] - E[\eta_{IE}\eta_{EL}])}{8S^2T^2(1-d/2)^2} = \frac{E[\eta_{IE}^2] - E[\eta_{IE}\eta_{EL}]}{4ST} \quad (28)$$

The above approximation is valid for SNR above -30 dB, which is typically the case for the GPS. If we incorporate (22)-(26), then (28) becomes

$$\begin{aligned} \text{Var}(\rho) = & \frac{P_n}{4ST} [dM + \sum_{i=1}^{K-Kd-1} (M-i)(1+d-i/K) \frac{\sin(i\pi B_f/B_s)}{i\pi B_f/B_s} \\ & + 2 \sum_{K-Kd}^{K-1} (M-i)(1-i/K) \frac{\sin(i\pi B_f/B_s)}{i\pi B_f/B_s} - \sum_{i=1}^{K+Kd-1} (M-i)(1-|Kd-i|/K) \frac{\sin(i\pi B_f/B_s)}{i\pi B_f/B_s}] \end{aligned} \quad (29)$$

The first summation in (29)

$$\begin{aligned} & \sum_{i=1}^{K-Kd-1} (M-i)(1+d-i/K) \frac{\sin(i\pi B_f/B_s)}{i\pi B_f/B_s} \\ & \approx \sum_{i=1}^{K-Kd-1} M(1+d-i/K) \frac{\sin(i\pi B_f/B_s)}{i\pi B_f/B_s} \end{aligned} \quad (30)$$

In the above equation,  $M-i$  is approximated by  $M$ , since the upper limit of the sum,  $K-Kd-1$ , is very small compared to  $M$ . We rewrite (30) as

$$\sum_{i=1}^{K-Kd-1} M(1+d-i/K) \frac{\sin(i\pi B_f/B_s)}{i\pi B_f/B_s} = \frac{1}{T_s} \sum_{i=1}^{K-Kd-1} M(1+d-i/K) \frac{\sin(i\pi B_f/B_s)}{i\pi B_f/B_s} T_s \quad (31)$$

where  $T_s$  is the sampling interval, and can be expressed in terms of the code chip width,  $T_c$ , as

$$T_s = \frac{T_c}{K} = \frac{T}{M} \quad (32)$$

If we set  $i = \frac{K}{T_c} t$ , then (31) can be written as

$$\frac{1}{T_s} \sum_{i=1}^{K-Kd-1} M(1+d-i/K) \frac{\sin(i\pi B_f/B_s)}{i\pi B_f/B_s} T_s \approx \frac{M}{T_s} \int_0^{(1-d)T_c} (1+d-t/T_c) \frac{\sin[t\pi B_f K/(B_s T_c)]}{t\pi B_f K/(B_s T_c)} dt \quad (33)$$

Using the relationships in (27),

$$\begin{aligned}
& \frac{M}{T_s} \int_0^{(1-d)T_c} (1+d-t/T_c) \frac{\sin[t\pi B_f K / (B_s T_c)]}{t\pi B_f K / (B_s T_c)} dt \\
&= \frac{M}{T_s} \int_0^{(1-d)T_c} (1+d-t/T_c) \frac{\sin[t\pi B_f / (10^6 T_c)]}{t\pi B_f / (10^6 T_c)} dt \\
&= \frac{KM}{T_c} \int_0^{(1-d)T_c} (1+d-t/T_c) \frac{\sin[t\pi B_f / (10^6 T_c)]}{t\pi B_f / (10^6 T_c)} dt \\
&= A_1 MK
\end{aligned} \tag{34}$$

where  $A_1$  is a constant, independent of  $K$ . Similarly, the other two terms of the summation in (29) can also be simplified as  $A_2 KM$  and  $A_3 KM$ , where  $A_2$  and  $A_3$  are constants. Thus, (29) can be written as

$$\text{Var}(\rho) = \frac{P_n M}{4ST} [d + (A_1 + A_2 + A_3)K] \tag{35}$$

We substitute (24) into (35), with  $P_n = N_0 B_f T / M$ ,

$$\text{Var}(\rho) = \frac{N_0 B_f T}{4ST} M [d + (A_1 + A_2 + A_3)K] = \frac{N_0 B_f}{4S} [d + (A_1 + A_2 + A_3)K] \tag{36}$$

Therefore, the tracking error variance increases for increased sampling rate. This change is linear.

Another common approach to evaluate the discriminator performance deals with the discriminator error. In this case, the error value is the discriminator non-zero output at synchronization. Compared with the tracking error, which is expressed in time, the discriminator error is analyzed in amplitude. It is straightforward to show that the variance of discriminator error can be expressed as

$$\text{Var}(D|_{t_p=0}) = 16ST(1-d/2)^2 (E[\eta_{IE}^2] - E[\eta_{IE}\eta_{IL}]) + 8(E^2[\eta_{IE}^2] - E^2[\eta_{IE}\eta_{IL}]) \tag{37}$$

By examining both error variance expressions, we find that the reduction of correlator spacing decreases the error variance. The error variance can also be lowered by decreasing the sampling rate. However, as discussed in the previous section, the sampling rate itself is lower bounded with a value decided by the correlator spacing. Figure 18 reveals the bound on the tracking error due to minimum sampling rate at different correlator spacing.

## 5. Simulation Results

In this section, we present the results obtained from 20,000 Monte Carlo trials, generated based on the non-Gaussian noise models described in section 2. The objective is to estimate the effects of noise, the precorrelation filter bandwidth, and sampling rate on GPS receiver performance, specifically on the early-late discriminator tracking error variance. We compare the analytical expressions of the tracking error variance derived in Section 4 with the simulation results. The first set of simulation demonstrates the relationship between the precorrelation filter bandwidth and both the tracking error variance and the discriminator variance. The second set of simulations shows the discriminator statistics in terms of the sampling rate.

First, we compute the values of discriminator tracking error variance over a range of precorrelation filter bandwidths between 2 and 10 MHz. The sampling rate is fixed at 30 samples per chip, and the early-late correlator spacing is set to 0.4 chips. All non-Gaussian noise models discussed in Section 2 are considered and have given almost identical results. The SNR is set to -30 dB. Figure 19 shows that the tracking error variance increases as the precorrelation filter bandwidth increases. The simulations follow very closely the analytical results of equations (28) and (37). Increasing the filter bandwidth beyond that of the GPS reduces the noise correlation, but at the same time allows more noise into the discriminator. These competing forces are responsible for almost the constant behavior over the range 4-6 MHz. However, the figure shows that a large precorrelation filter bandwidth generally compromises the discriminator performance, irrespective of the noise statistics. We also simulate the discriminator error variance versus the precorrelation filter bandwidth, which is shown in Figure 20. The result is consistent with that of the tracking error.

The second set of simulations considers the noise models of Section 2. Figure 21 shows the different values of discriminator tracking error variance with a range of sampling rates between 5 and 30 samples per chip, under SNR of -30 dB. The precorrelation filter bandwidth is fixed as 2 MHz and the early-late correlator spacing is set to 0.4 chips. We find that the tracking error variance increases as the

sampling rate increases. The analytical and simulation curves in Figure 21 are very close and both demonstrate linear behavior. Figure 22 shows the relationship between the discriminator error variance and the sampling rate, which gives the same result.

Figure 23 provides the tracking error variance with 2 MHz precorrelation filter bandwidth and 30 samples per chip over a range of SNR between -50 dB and 10 dB. It is clear that the simulation result tracking error variance is very close to its theoretical counterpart of (28) at SNR above -30 dB.

## 6. Conclusions

This chapter has dealt with the effect of non-Gaussian noise on GPS receiver performance. It was shown that long time-averaging featured in the GPS DLL is responsible for producing Gaussian noise. We considered the error variance of the early-late discriminator which is induced by the correlator noise components of impulsive noise, UWB signals, and noise radar signals. Both expressions of the tracking error variance (time) and the discriminator variance (amplitude) in noise are derived. The results show that the DLL discriminator statistics are highly dependent on the precorrelation filter bandwidth, the sampling rate, the early-late correlator spacing, and the SNR. The precorrelation filter plays a key role of changing the correlation between noise samples, which subsequently affects the error variance of discriminator. Higher sampling rates increase noise sample correlations, which leads to increased discriminator tracking errors. Lowering the number of samples per chip is, however, bounded by the early-late correlator spacing. These competing requirements as well as the tradeoff between noise correlation and noise power, as a result of increasing filter bandwidth, are analyzed and verified by computer simulations.

## APPENDIX A

First, we discuss the statistics of the correlator noise components  $\eta_{IE}$ ,  $\eta_{IL}$ ,  $\eta_{IP}$ ,  $\eta_{QE}$ ,  $\eta_{QL}$ , and  $\eta_{QP}$  from (16). We note that,

$$\begin{aligned}
E[\eta_{IE}^2] &= E\left[\left(\sum_{\ell=1}^M n(\ell)g(\ell)\right)^2\right] \\
&= E\left[\sum_{\ell=1}^M (n(\ell)g(\ell))^2 + 2n(1)g(1)\sum_{\ell=2}^M n(\ell)g(\ell) + 2n(2)g(2)\sum_{\ell=3}^M n(\ell)g(\ell) \right. \\
&\quad \left. + \dots + 2n(M-1)g(M-1)n(M)g(M)\right]
\end{aligned} \tag{A1}$$

where  $n(\ell)$  represents the noise sample,  $g(\ell)$  is the C/A code sample, and  $M$  is the total number of samples. Since  $n(\ell)$  and  $g(\ell)$  are independent, (A1) becomes

$$\begin{aligned}
E[\eta_{IE}^2] &= E\left[\left(\sum_{i=1}^M n(i)g(i)\right)^2\right] \\
&= \sum_{\ell=1}^M E[(n(\ell)^2)E[g(\ell)^2]] + 2\sum_{\ell=2}^M E[n(1)n(\ell)]E[g(1)g(\ell)] + 2\sum_{\ell=3}^M E[n(2)n(\ell)]E[g(2)g(\ell)] \\
&\quad + \dots + 2E[n(M-1)n(M)]E[g(M-1)g(M)]
\end{aligned} \tag{A2}$$

For simplification, we use

$$R_f(r) = E[g(a)g(a+r)] = 1 - r/K \text{ for } r = 0, 1, 2, \dots, K-1; \quad R_f(r) = 0 \text{ for } r = K, K+1, \dots, M \tag{A3}$$

to approximate the correlation function between the filtered and the reference C/A code, and

$$R_{fn}(r) = E[n(a)n(a+r)]P_n \frac{\sin(r\pi B_f / B_s)}{r\pi B_f / B_s} \tag{A4}$$

to approximate the noise correlation function. Thus, (A2) becomes

$$E[\eta_{IE}^2] = P_n \left[ M + 2\sum_{r=1}^{K-1} (M-r)(1-r/K) \frac{\sin(r\pi B_f / B_s)}{r\pi B_f / B_s} \right] \tag{A5}$$

where the total number of samples  $M = 1023k$ . Similarly,

$$E[\eta_{IE}^2] = E[\eta_{IL}^2] = E[\eta_{IP}^2] = E[\eta_{QE}^2] = E[\eta_{IL}^2] = E[\eta_{IP}^2] \tag{A6}$$

Moreover,

$$E[\eta_{IE}\eta_{IL}] = E\left[\left(\sum_{\ell=1}^M n(\ell)g(\ell)\right)\left(\sum_{\ell=1}^M n(\ell)g(\ell + Kd)\right)\right]$$

$$\begin{aligned}
&= E\left[\sum_{\ell=1}^M n(\ell)g(\ell)n(\ell)g(\ell + Kd)\right] + E\left[n(1)g(1)\sum_{\ell=2}^M n(\ell)g(\ell + Kd)\right] \\
&+ n(2)g(2)\sum_{\ell=3}^M n(\ell)g(\ell + Kd) + \cdots + n(M-1)g(M-1)n(M)g(M + Kd)] \\
&+ E\left[n(2)g(2)n(1)g(1 + Kd) + n(3)g(3)\sum_{\ell=1}^2 n(\ell)g(\ell + Kd) + \cdots + n(M)g(M)\sum_{\ell=1}^{M-1} n(\ell)g(\ell + Kd)\right] \\
&= \sum_{\ell=1}^M E[n(\ell)n(\ell)]E[g(\ell)g(\ell + Kd)] + \sum_{\ell=2}^M E[n(1)n(\ell)]E[g(1)g(\ell + Kd)] \\
&+ \sum_{\ell=3}^M E[n(2)n(\ell)]E[g(2)g(\ell + Kd)] + \cdots + E[n(M-1)n(M)]E[g(M-1)g(M + Kd)] \\
&+ E[n(2)n(1)]E[g(2)g(1 + Kd)] + \sum_{\ell=1}^2 E[n(3)n(\ell)]E[g(3)g(\ell + Kd)] + \cdots + \sum_{\ell=1}^{M-1} E[n(M)n(\ell)]E[g(M)g(\ell + Kd)] \\
&= P_n \left\{ (1-d)M + \sum_{r=1}^{K-Kd-1} (M-r)(1-d-r/K) \frac{\sin(r\pi B_f / B_s)}{r\pi B_f / B_s} \right. \\
&\left. + \sum_{r=1}^{K+Kd-1} (M-r)(1-|Kd-r|/K) \frac{\sin(r\pi B_f / B_s)}{r\pi B_f / B_s} \right\} \tag{A7}
\end{aligned}$$

where  $d$  is the early-late correlator spacing measured in chips.

Next, we derive the expression of discriminator tracking error variance, assuming the tracking error is confined into the linear working range of discriminator function. From (15),

$$\begin{aligned}
D &= (I_E^2 + Q_E^2) - (I_L^2 + Q_L^2) \\
&= (\sqrt{2STR}(\tau_E) \cos \varphi + \eta_{IE})^2 + (\sqrt{2STR}(\tau_E) \sin \varphi + \eta_{QE})^2 \\
&- (\sqrt{2STR}(\tau_L) \cos \varphi + \eta_{IL})^2 - (\sqrt{2STR}(\tau_L) \sin \varphi + \eta_{QL})^2 \\
&= \{\sqrt{2ST} \cos(\varphi)[1 - (\rho + d/2)] + \eta_{IE}\}^2 + \{\sqrt{2ST} \sin(\varphi)[1 - (\rho + d/2)] + \eta_{QE}\}^2 \\
&- \{\sqrt{2ST} \cos(\varphi)[1 + (\rho - d/2)] + \eta_{IL}\}^2 - \{\sqrt{2ST} \sin(\varphi)[1 + (\rho - d/2)] + \eta_{QL}\}^2
\end{aligned} \tag{A8}$$

where  $\rho$  is the time delay of C/A code autocorrelation function and  $d$  is the early-late correlator spacing.

When  $D = 0$ , the tracking error

$$\rho = \frac{\eta_{IE}^2 + \eta_{QE}^2 - \eta_{IL}^2 - \eta_{QL}^2 + 2\sqrt{2ST}(1-d/2)[(\eta_{IE} - \eta_{IL}) \cos \varphi + (\eta_{QE} - \eta_{QL}) \sin \varphi]}{8ST(1-d/2)} \tag{A9}$$

Because of the zero mean of all the correlator noise components and (A6),

$$E[\rho] = 0 \tag{A10}$$

Thus, the tracking error variance

$$\text{Var}(\rho) = E[\rho^2] - (E[\rho])^2 = E[\rho^2] \quad (\text{A11})$$

We have validated that all correlator noise components  $\eta_{IE}$ ,  $\eta_{IL}$ ,  $\eta_{QE}$  and  $\eta_{QL}$  are Gaussian. Taking advantage of Gaussian Joint-Variable Theorem,

$$E[\eta_1\eta_2\eta_3\eta_4] = E[\eta_1\eta_2]E[\eta_3\eta_4] + E[\eta_1\eta_3]E[\eta_2\eta_4] + E[\eta_1\eta_4]E[\eta_2\eta_3] \quad (\text{A12})$$

Using the above expression, it is straightforward to show that

$$\text{Var}(\rho) = \frac{(E[\eta_{IE}^2])^2 - (E[\eta_{IE}\eta_{EL}])^2 + 2ST(1-d/2)^2(E[\eta_{IE}^2] - E[\eta_{IE}\eta_{EL}])}{8S^2T^2(1-d/2)^2} \quad (\text{A13})$$

Finally, we present the derivation of the discriminator error variance expression. At the point of synchronization, we have

$$R(\tau_E) = R(\tau_L) = 1 - d/2; \quad (\text{A14})$$

From (15), the discriminator output is

$$\begin{aligned} D|_{\rho=0} &= (I_E^2 + Q_E^2) - (I_L^2 + Q_L^2) \\ &= (\sqrt{2STR}(\tau_E)\cos\phi + \eta_{IE})^2 + (\sqrt{2STR}(\tau_E)\sin\phi + \eta_{QE})^2 \\ &\quad - (\sqrt{2STR}(\tau_L)\cos\phi + \eta_{IL})^2 - (\sqrt{2STR}(\tau_L)\sin\phi + \eta_{QL})^2 \\ &= [\sqrt{2ST}\cos\phi(1-d/2) + \eta_{IE}]^2 + [\sqrt{2ST}\sin\phi(1-d/2) + \eta_{QE}]^2 \\ &\quad - [\sqrt{2ST}\cos\phi(1-d/2) + \eta_{IL}]^2 - [\sqrt{2ST}\sin\phi(1-d/2) + \eta_{QL}]^2 \\ &= \eta_{IE}^2 + \eta_{QE}^2 - \eta_{IL}^2 - \eta_{QL}^2 + 2\sqrt{2ST}(1-d/2)[\cos\phi(\eta_{IE} - \eta_{IL}) + \sin\phi(\eta_{QE} - \eta_{QL})] \end{aligned} \quad (\text{A15})$$

It's evident that

$$E[D|_{\rho=0}] = 0 \quad (\text{A16})$$

The discriminator error variance is

$$\begin{aligned} \text{Var}(\rho) &= E[D|_{\rho=0}] - (E[D|_{\rho=0}])^2 = E[D|_{\rho=0}^2] \\ &= 16ST(1-d/2)^2(E[\eta_{IE}^2] - E[\eta_{IE}\eta_{IL}]) + 8(E^2[\eta_{IE}^2] - E^2[\eta_{IE}\eta_{IL}]) \end{aligned} \quad (\text{A17})$$

## References

- [1] W. Zhuang and J. Tranquilla, "Modeling and analysis for the GPS pseudo-range observable", *IEEE Transactions on Aerospace and Electronic Systems*, vol. 31, No. 2, pp. 739-751, April 1995.
- [2] M. S. Braasch, "Autocorrelation sidelobe consideration in the characterization of multipath errors", *IEEE Transactions on Aerospace and Electronic Systems*, vol. 33, No.1, pp. 290-295, Jan. 1997.
- [3] R. L. Fante and J. J. Vaccaro, "Evaluation and reduction of multipath-induced bias on GPS time-of-arrival", *IEEE Transactions on Aerospace and Electronic Systems*, vol. 39, No. 3, pp. 911-920, July 2003.
- [4] J. W. Erickson, P. S. Maybeck, and J. F. Raquet, "Multipath-adaptive GPS/INS receiver", *IEEE Transactions on Aerospace and Electronic Systems*, vol. 41, Issue 2, pp. 645-657, April 2005.
- [5] J. Soubielle, I. Fijalkow, P. Duvaut, and A. Bibaut, "GPS positioning in a multipath environment", *IEEE Transactions on Signal Processing*, vol. 50, Issue 1, pp. 141-150, Jan. 2002.
- [6] M. G. Amin, L. Zhao, and A. R. Lindsey, "Subspace array processing for the suppression of FM jamming in GPS receivers", *IEEE Transactions on Aerospace and Electronic Systems*, vol. 40, Issue 1, pp. 80-92, Jan. 2004.
- [7] M. G. Amin and W. Sun, "A novel interference suppression scheme for global navigation satellite systems using antenna array", *IEEE Journal on Selected Areas in Communications*, vol. 23, Issue 5, pp. 999-1012, May 2005.
- [8] P. H. Mdhani, P. Axelrad, K. Krumvieda, and J. Thomas, "Application of successive interference cancellation to the GPS pseudolite near-far problem", *IEEE Transactions on Aerospace and Electronic Systems*, vol. 39, Issue 2, pp. 481-488, April 2003.
- [9] S. Yoon, L. Song, and S. Y. Kim, "Code acquisition for DS/SS communications in non-Gaussian impulsive channels", *IEEE Transactions on Communications*, vol. 52, Issue 2, pp. 187-190, Feb. 2004.
- [10] Q. Wu, "A study of automobile electromagnetic disturbance of noise source", *1997 International Symposium on Electromagnetic Compatibility Proc.*, pp. 199-202, 21-23 May 1997.
- [11] N. Dawood and R. M. Narayanan, "Receiver operating characteristics for the coherent UWB random noise radar", *IEEE Transactions on Aerospace and Electronic Systems*, vol. 37, Issue 2, pp. 586-594, April 2001.
- [12] P. A. Dafesh, P. Hanson, R. Yowell, T. Stansell and D. Alcocer, "A portable UWB to GPS emission simulator", *Position Location and Navigation Symposium 2004*, pp. 405-413, April 26-29, 2004.
- [13] Q. Zeng, "Suitability of some propagation models to analyse interference from ultra wideband transmitters in outdoor environments", *2003 IEEE Conference on Ultra Wideband Systems and Technologies*, pp. 488-492, Nov. 16-19, 2003.
- [14] S. Nag, H. Fluhler, and M. Barnes, "Preliminary Interferometric Images of Moving Targets obtained using a Time-Modulated Ultra-Wide Band Through-Wall Penetration Radar", *Proc. IEEE Radar Conference*, pp. 64-69, May 2001.

- [15] J. Z. Tatoi, G. Franceschetti, H. Lackner, and G. Gibbs, "Through-the-Wall Impulse SAR Experiments", Digest of the 2005 IEEE AP-S International Symposium/USNC/URSI National Radio Science Meeting (APS/URSI 2005), July 3-8, 2005, Washington DC, USA.
- [16] D. Cassioli, M. Z. Win, and A. F. Molisch, "The ultra-wide bandwidth indoor channel: from statistical model to simulations", IEEE Journal on Selected Areas in Communications, vol. 20, Issue 6, pp. 1247-1257, Aug. 2002.
- [17] S. Cezici, H. Kobayashi, H. V. Poor, and A. F. Molisch, "Performance evaluation of impulse radio UWB systems with pulse-based polarity randomization", IEEE Transactions on Signal Processing, vol. 53, Issue 7, pp. 2537-2549, July 2005.
- [18] E. fishler and H. V. Poor, "Low-complexity multiuser detector for time-hopping impulse-radio systems", IEEE Transactions on Signal Processing, vol. 52, Issue 9, pp. 2561-2571, Sept. 2004.
- [19] D. Apostolakis and P. Constantinou, "Man made noise measurements and modelling", 'Personal Communications: Gateway to the 21st Century' Conference Record, 2nd International Conference, vol. 2, pp. 585, Oct. 1993.
- [20] W. R. Lauber and J. M. Bertrand, "Statistics of motor vehicle ignition noise at VHF/UHF", IEEE Transactions on Electromagnetic Compatibility, vol. 41, No. 3, pp. 257-259, Aug. 1999.
- [21] S. M. Zabin and H. V. Poor, "Parameter estimation for Middleton Class A interference processes", IEEE Transactions on Communications, vol. 37, No. 10, Oct 1989.
- [22] S. A. Kassam, Signal Detection in Non-Gaussian Noise, pp. 74-90, Dowden & Culver, Inc., New York, 1988.
- [23] C. L. Nikias and M. Shao, Signal processing with alpha-stable distributions and applications, John Wiley & Sons, Inc., pp.16, 1995.
- [24] D. Apostolakis and P. Constantinou, "Man made noise measurements and modelling", 'Personal Communications: Gateway to the 21st Century' Conference Record, 2nd International Conference, vol. 2, pp. 586-588, Oct. 1993.
- [25] J. Hoffman and M. Cotton, "Measurements to determine potential interference to GPS ultrawideband transmission systems", NTIA Report 01-384, Feb. 2001.
- [26] M. Sahnoudi, K. Abed-Meraim, and M. Benidir, "Blind separation of impulsive alpha-stable sources using minimum dispersion criterion", IEEE Signal Processing Letters, vol. 12, No. 4, pp. 281-284, April 2005.
- [27] K. Mizutani, D. Umehara, M. Kawai, and Y. Morihira, "Noncoherent FSK optimum receiver over impulsive noise channels", Proc. of the 7th International Symposium on Power-Line Communications and Its Applications, Kyoto, Japan, pp. 91, March 26-28, 2003.
- [28] D. Cassioli, M. Z. Win, and A. F. Molisch, "The ultra-wide bandwidth indoor channel: from statistical model to simulations", IEEE Journal on Selected Areas in Communications, vol. 20, No. 6, Aug. 2002.

[29] J. Kurnisch and J. Pamp, "An ultra-wideband space-variant multipath indoor radio channel model", 2003 IEEE Conference on Ultra Wideband Systems and Technologies, pp. 290-294, 16-19 Nov. 2003.

[30] Q. T. Zhang and S. H. Song, "Parsimonious correlated non-stationary models for real UWB data", IEEE International Conference on Communications, vol. 6, pp. 3419-3423, 20-24 June 2004.

[31] A. J. Van Dierendonck, P. Fenton, and T. Ford, "Theory and performance of narrow correlator spacing in a GPS receiver", Navigation: Journal of the Institute of Navigation, vol. 39, No. 3, pp. 281, Fall 1992.

[32] B. Parkinson and J. Spilker Jr., Global Positioning System: Theory and Applications Volume I, pp. 363-364, American Institute of Aeronautics and Astronautics, Inc., Washington, 1996.

## Tables and Figures

Table 1. Delay bias from different precorrelation filter bandwidth

Filter bandwidth (MHz)	Phase bias (chips)
2	1.06
3	0.72
4	0.53
5	0.43
6	0.36
7	0.31
8	0.27
9	0.23
10	0.21

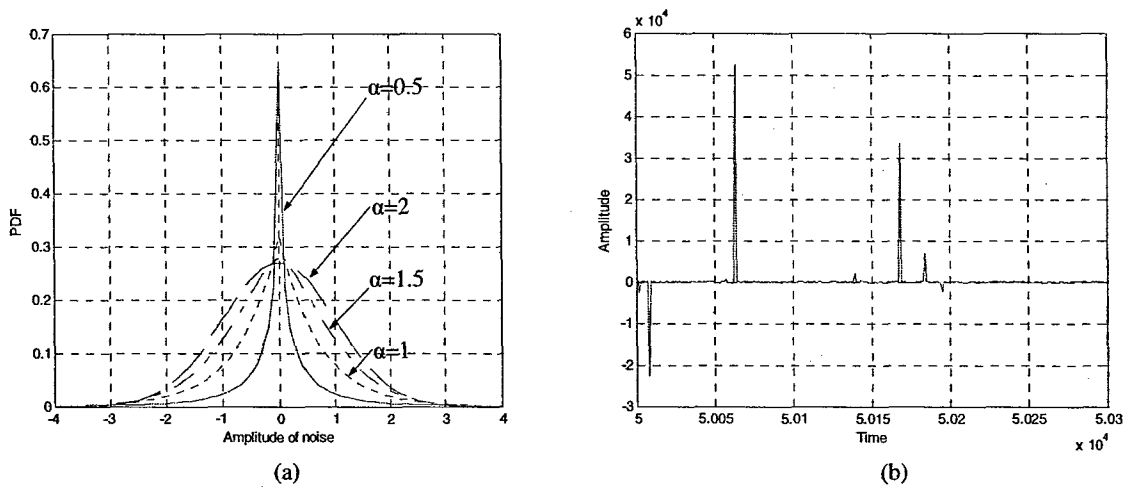


Figure 1 (a) PDF of SaS noise model, (b) Sample sequence of SaS noise

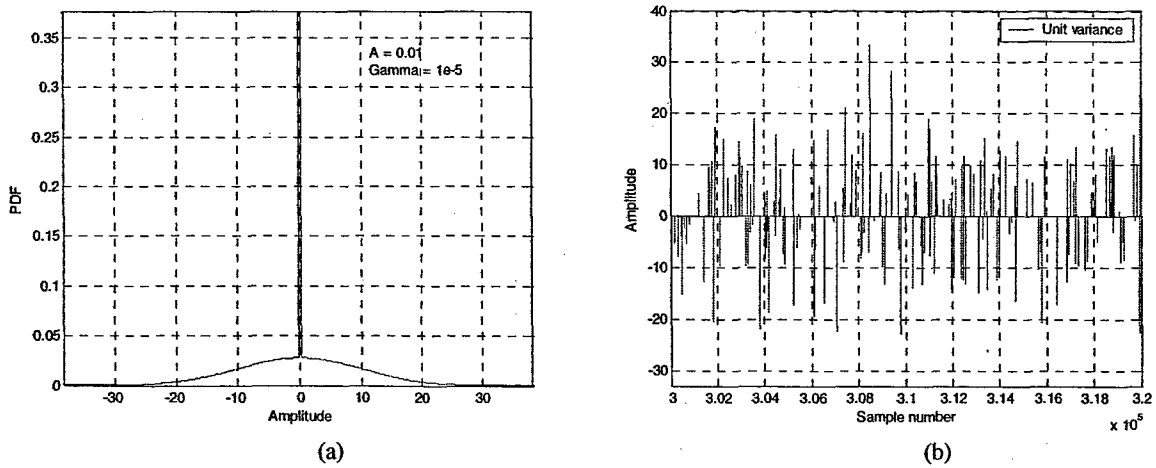
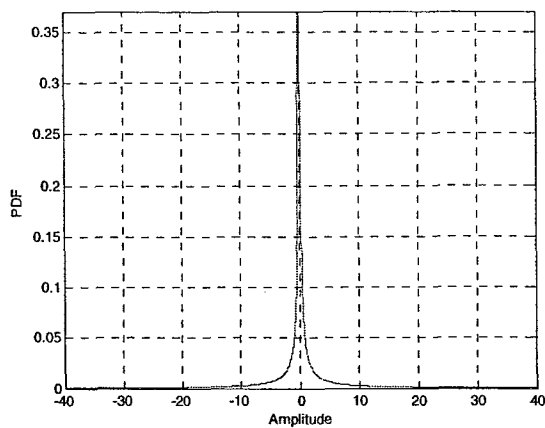
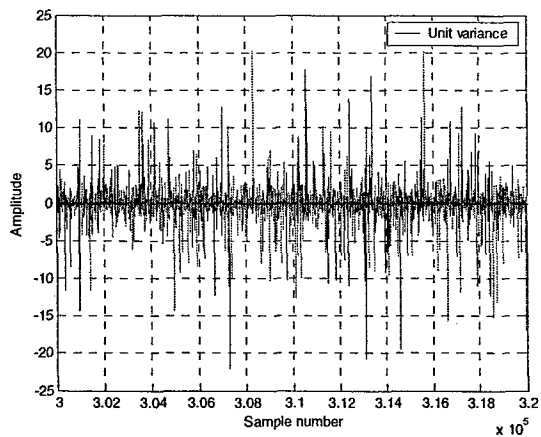


Figure 2 (a) PDF of the simplified Middleton noise model, (b) Sample sequence of Middleton noise with unit variance

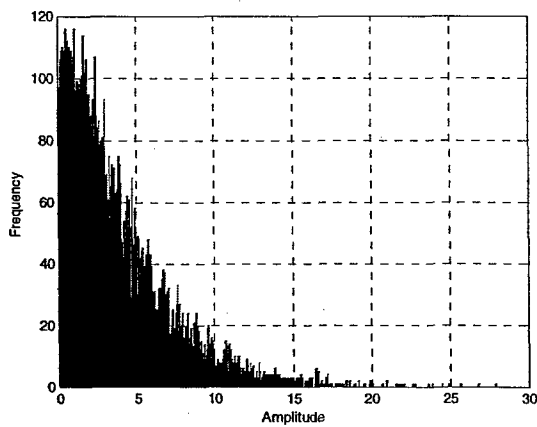


(a)

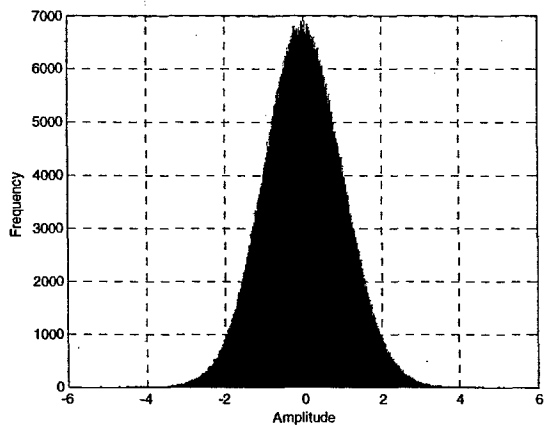


(b)

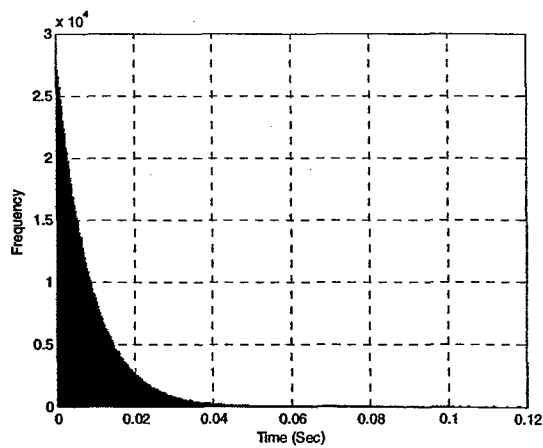
Figure 3 (a) PDF of generalized Cauchy noise model, (b) Sample sequence of Generalized Cauchy noise with unit variance



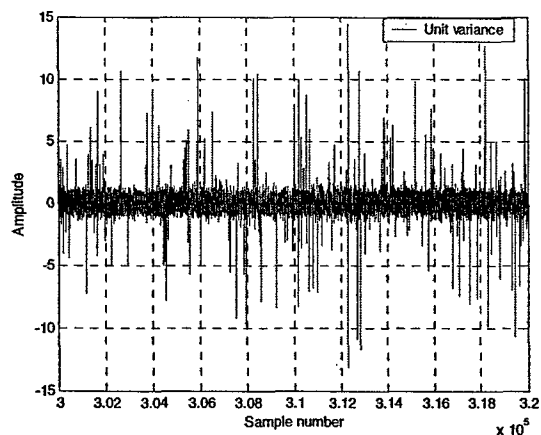
(a)



(b)

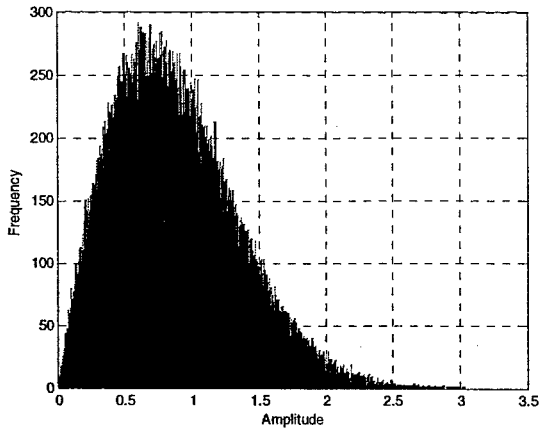


(c)

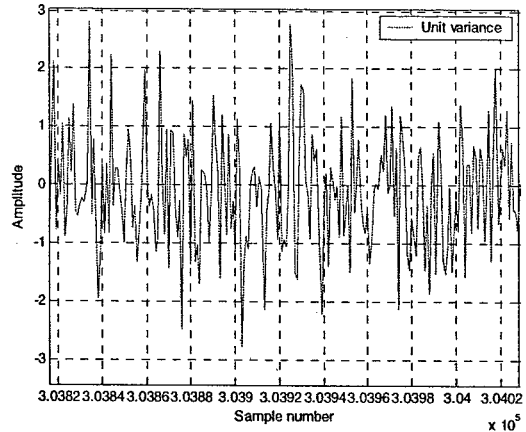


(d)

Figure 4 (a) PDF of the power peaks, (b) PDF of the low power values, (c) PDF of the inter-arrival times between successive peaks, (d) Sample sequence of ignition noise with unit variance

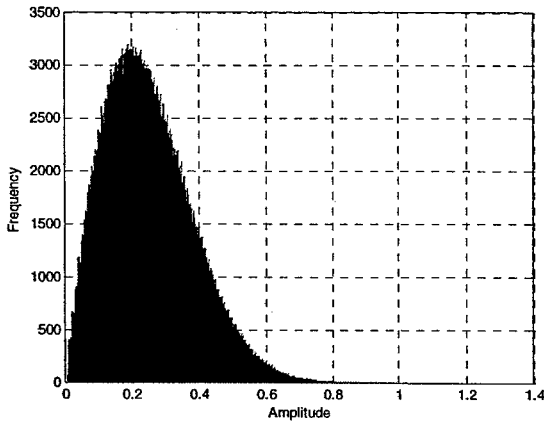


(a)

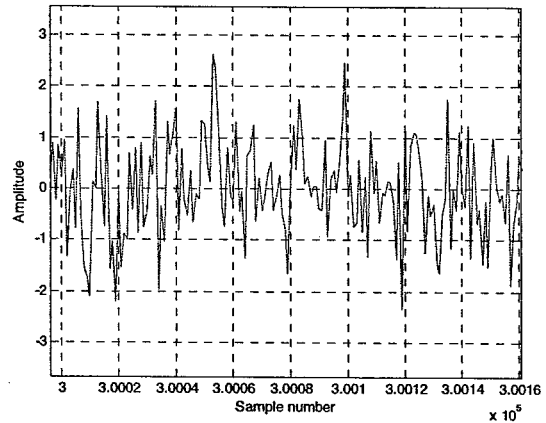


(b)

Figure 5 (a) PDF of the amplitude of aggregate UWB signals, (b) Sample sequence of UWB noise with unit variance



(a)



(b)

Figure 6 (a) PDF of the amplitude of noise radar signals, (b) Sample sequence of radar noise with unit variance

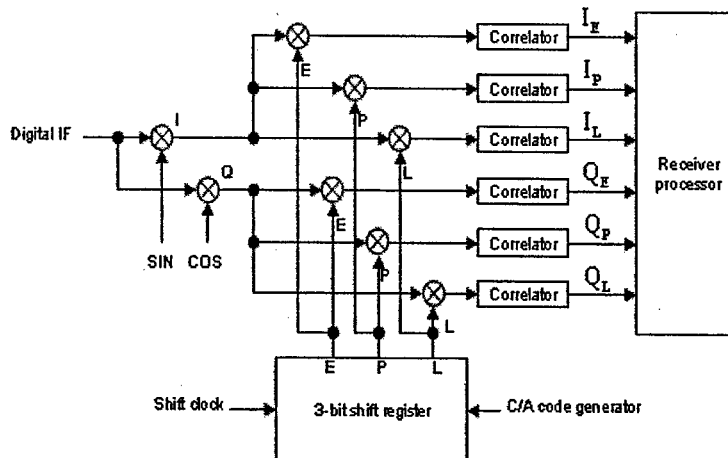
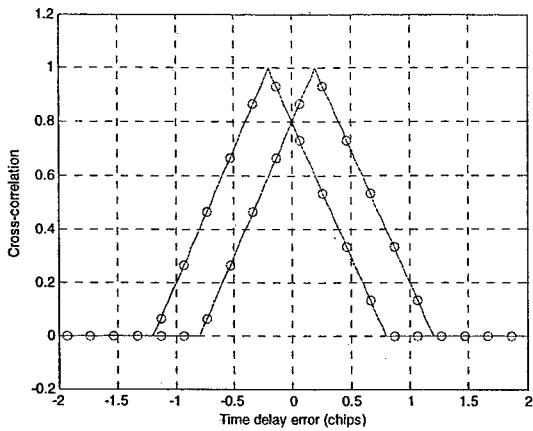
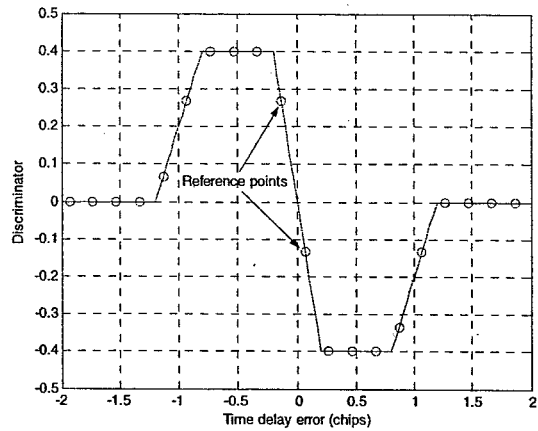


Figure 7 GPS DLL cross-correlation process

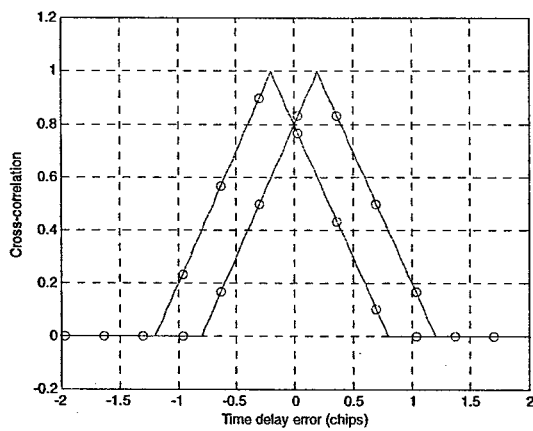


(a)

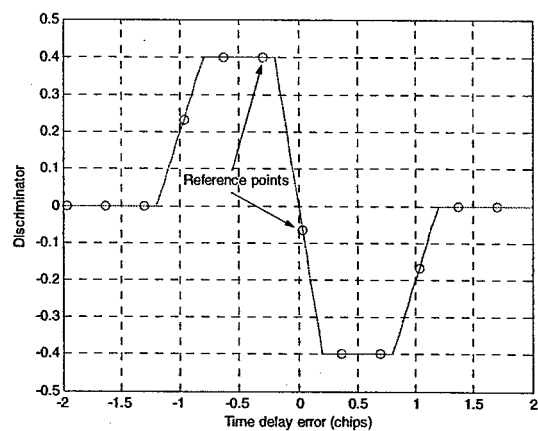


(b)

Figure 8 (a) Early-late correlation functions, (b) Discriminator function with 0.4-chip spacing and 5 samples per chip

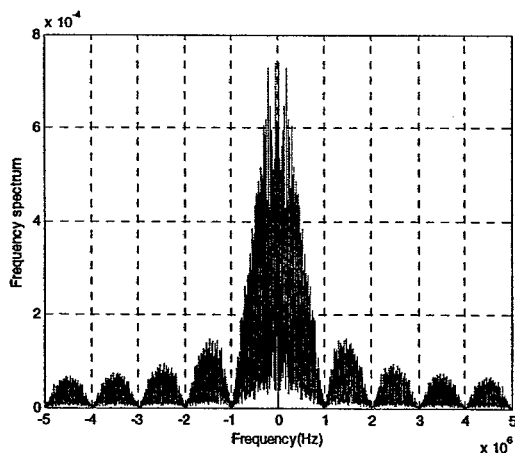


(a)

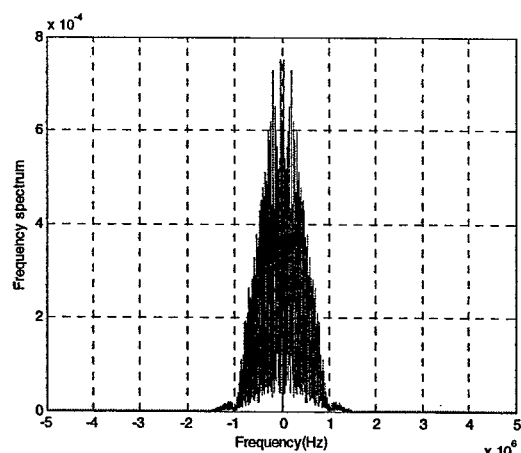


(b)

Figure 9 (a) Early-late correlation functions, (b) Discriminator function with 0.4-chip spacing and 4 samples per chip



(a)



(b)

Figure 10 The frequency spectrum of C/A code with 2 MHz bandwidth Butterworth precorrelation filtering (a) before filtered, (b) after filtered

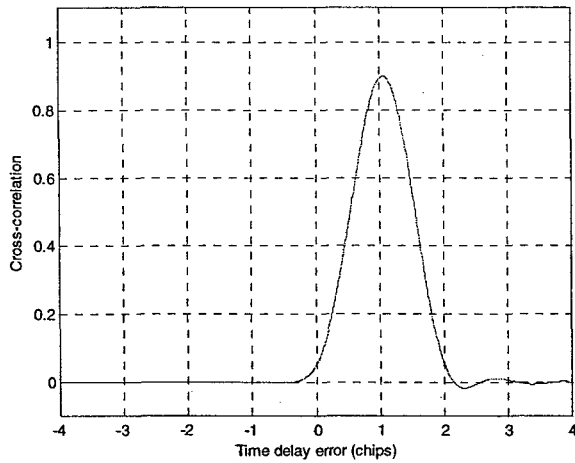


Figure 11 Cross-correlation between filtered C/A code and original C/A code

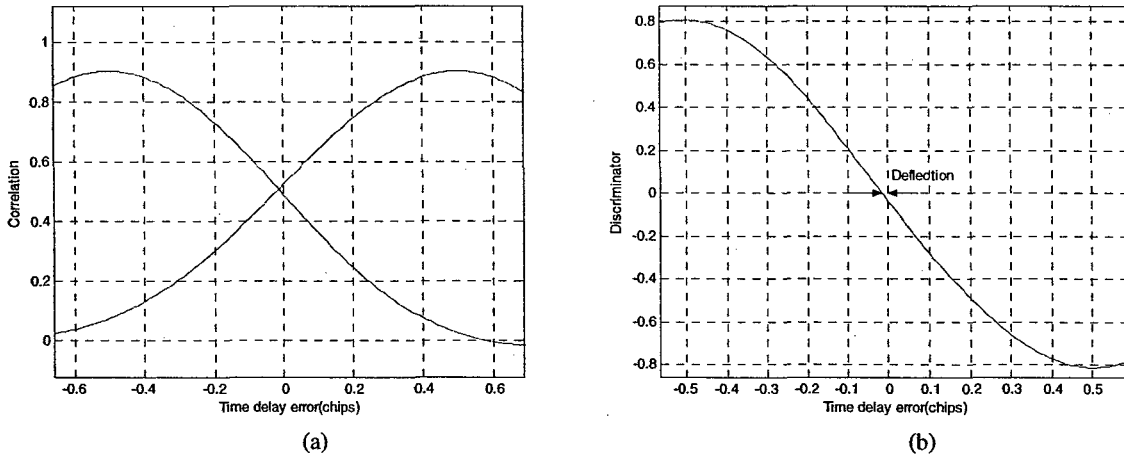


Figure 12 (a) Early-late correlation functions, (b) Discriminator function with 1 chip spacing and 2 MHz precorrelation filtering

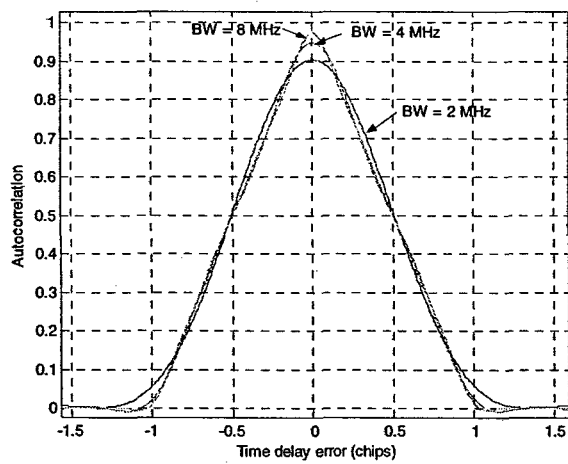
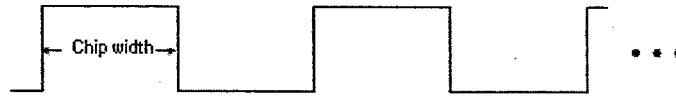


Figure 13 C/A code autocorrelation function after precorrelation filtering

C/A code



Noise samples

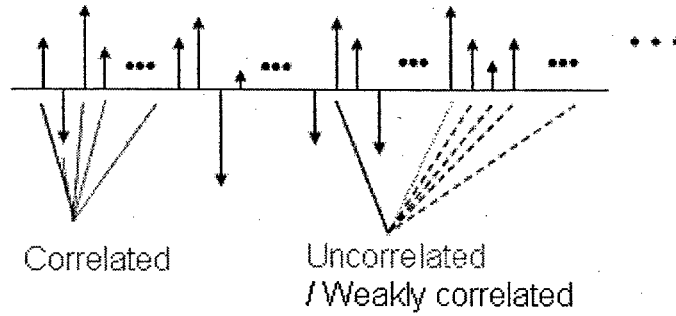
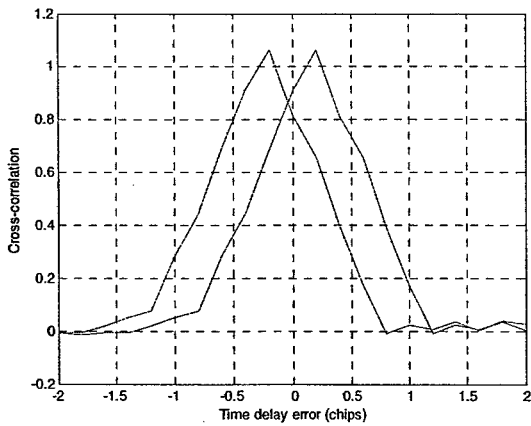
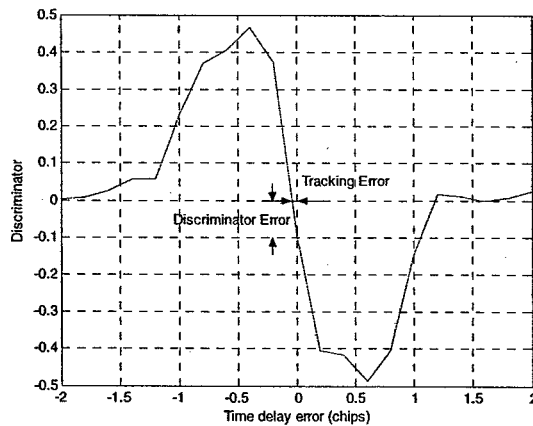


Figure 14 Correlation between noise samples with 1 MHz precorrelation filtering

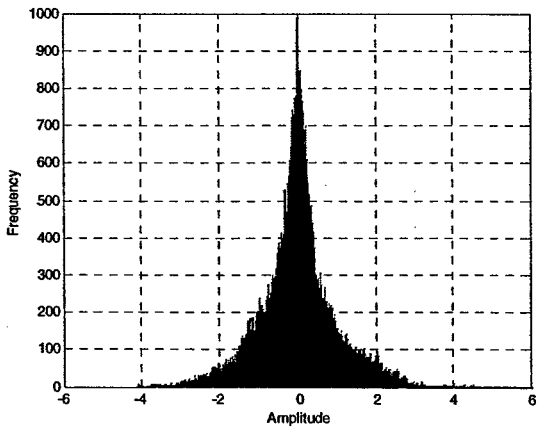


(a)

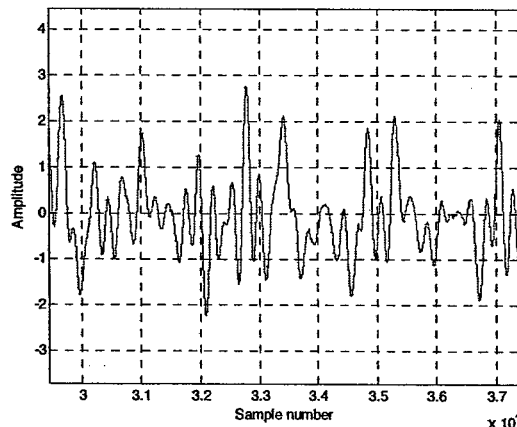


(b)

Figure 15 (a) Early-late correlation functions, (b) Discriminator function with 1 chip spacing and 2 samples per chip under -10 dB impulsive noise



(a)



(b)

Figure 16 (a) PDF of the filtered Middleton noise, (b) Sample sequence the filtered Middleton noise

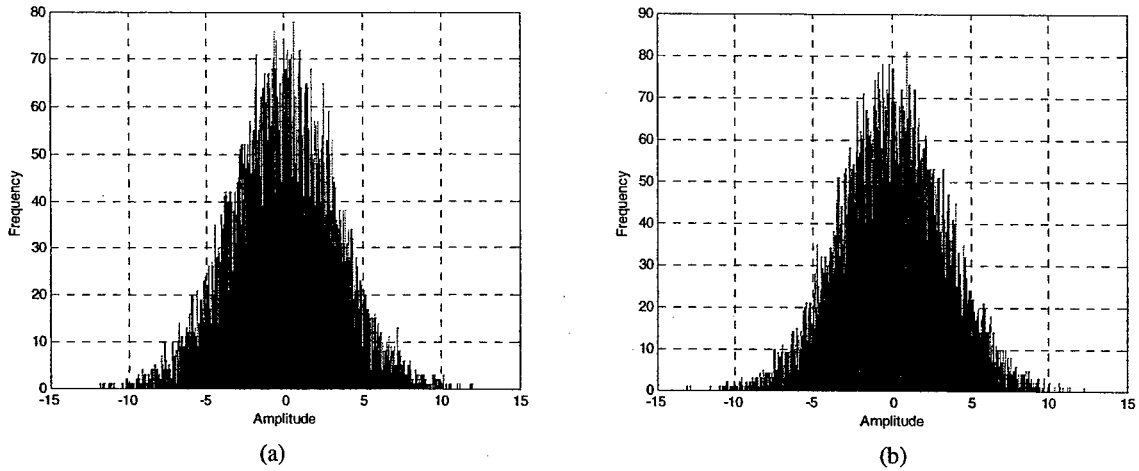


Figure 17 (a) PDF of correlator in-phase noise samples, (b) PDF of correlator quadrature noise samples

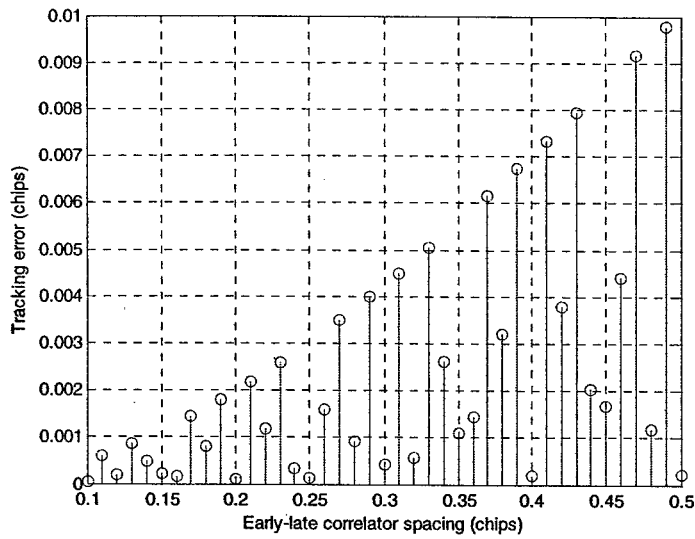


Figure 18 Minimal tracking error with 2 MHz bandwidth precorrelation filter

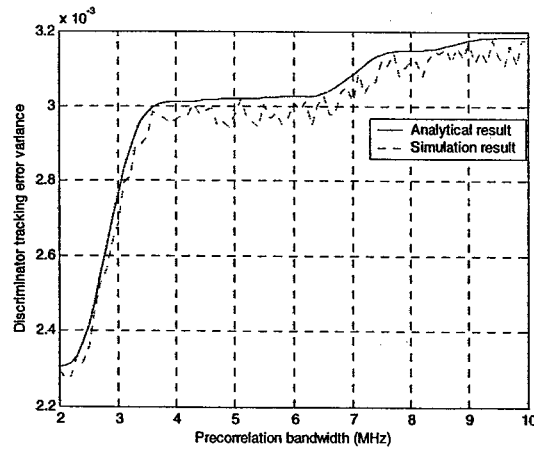


Figure 19 Discriminator tracking error variance through different bandwidth precorrelation filter under non-Gaussian noise

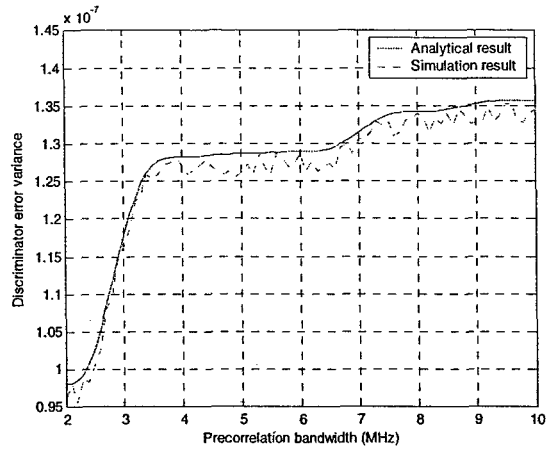


Figure 20 Discriminator error variance through different bandwidth precorrelation filter under non-Gaussian noise

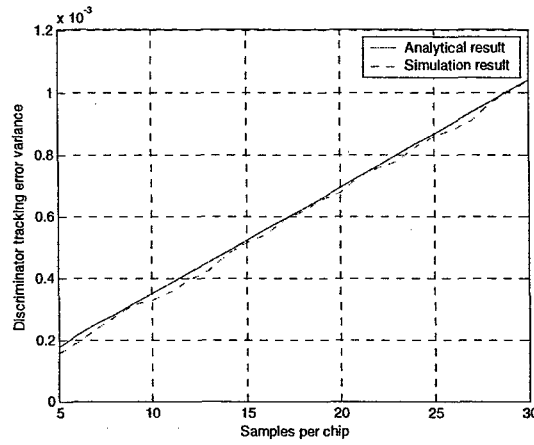


Figure 21 Discriminator tracking error variance with different sampling rate under non-Gaussian noise

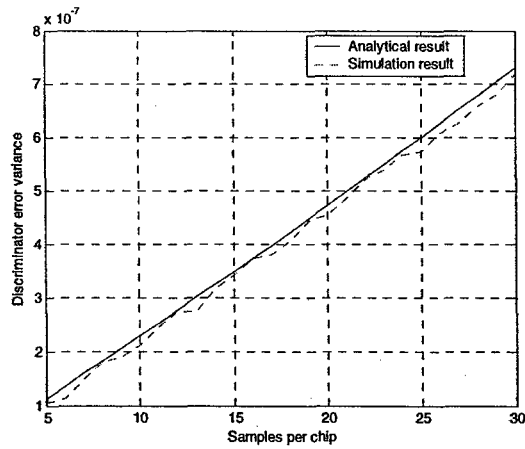


Figure 22 The discriminator error variance with different sampling rate under non-Gaussian noise

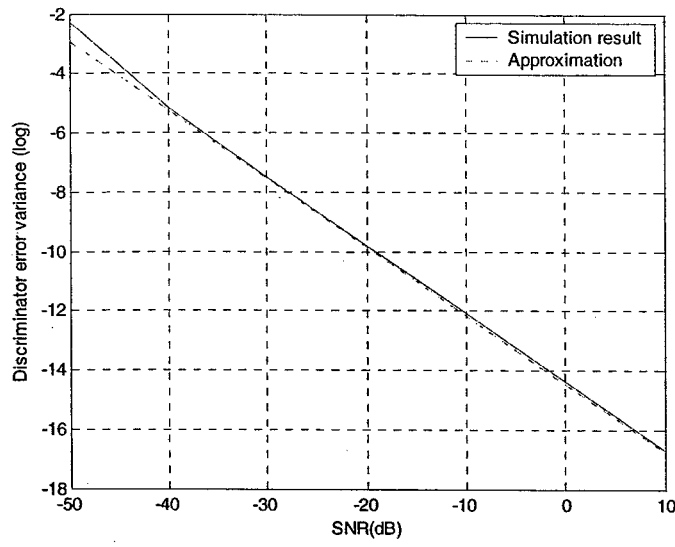


Figure 23 The approximation of discriminator tracking error variance at different SNR

**REPORT DOCUMENTATION PAGE**

*Form Approved*  
OMB No. 0704-0188

The public reporting burden for this collection of information is estimated to average 1 hour per response, including the time for reviewing instructions, searching existing data sources, gathering and maintaining the data needed, and completing and reviewing the collection of information. Send comments regarding this burden estimate or any other aspect of this collection of information, including suggestions for reducing the burden, to Department of Defense, Washington Headquarters Services, Directorate for Information Operations and Reports (0704-0188), 1215 Jefferson Davis Highway, Suite 1204, Arlington, VA 22202-4302. Respondents should be aware that notwithstanding any other provision of law, no person shall be subject to any penalty for failing to comply with a collection of information if it does not display a currently valid OMB control number.

**PLEASE DO NOT RETURN YOUR FORM TO THE ABOVE ADDRESS.**

<b>1. REPORT DATE (DD-MM-YYYY)</b> 15/09/2005		<b>2. REPORT TYPE</b> Final		<b>3. DATES COVERED (From - To)</b> June 2004 - September 2005	
<b>4. TITLE AND SUBTITLE</b> Array Processing for Interference Suppression in GPS Receivers				<b>5a. CONTRACT NUMBER</b>	
				<b>5b. GRANT NUMBER</b> N00014-04-1-0607	
				<b>5c. PROGRAM ELEMENT NUMBER</b>	
<b>6. AUTHOR(S)</b> Amin, Moeness G. (PI)				<b>5d. PROJECT NUMBER</b>	
				<b>5e. TASK NUMBER</b>	
				<b>5f. WORK UNIT NUMBER</b>	
<b>7. PERFORMING ORGANIZATION NAME(S) AND ADDRESS(ES)</b> Villanova University - Center for Advanced Communications 800 Lancaster Avenue - Tolentine 119 Villanova, PA 19085				<b>8. PERFORMING ORGANIZATION REPORT NUMBER</b> 5-27725	
<b>9. SPONSORING/MONITORING AGENCY NAME(S) AND ADDRESS(ES)</b> Office of Naval Research 875 N. Randolph Street 12th Floor, One Liberty Center Code 02 Arlington, VA 22217-5660				<b>10. SPONSOR/MONITOR'S ACRONYM(S)</b> ONR	
				<b>11. SPONSOR/MONITOR'S REPORT NUMBER(S)</b>	
<b>12. DISTRIBUTION/AVAILABILITY STATEMENT</b> Approved for Public Release; Distribution is Unlimited					
<b>13. SUPPLEMENTARY NOTES</b>					
<b>14. ABSTRACT</b> We examine the performance of the delay lock loops (DLL) in GPS receivers in the presence of non-Gaussian noise. Interference and noise sources for GPS receivers may assume Gaussian or non-Gaussian distributions, specifically when operating inside buildings. Non-Gaussian noise may contaminate the GPS satellite signals and compromise the receiver delay lock loops (DLL), producing significant tracking errors. These sources include impulsive noise, ultra-wideband (UWB) signals, and noise radar signals for target tracking and through-the-wall imaging applications. We have considered non-Gaussian noise and examined its effect on GPS correlation and discriminator outputs for the commercial GPS using Coarse Acquisition (C/A) code. The discriminator tracking error variance is derived, incorporating the effect of noise, the front-end precorrelation filter, and the sampling rate. Further, Interference suppression and multipath mitigation in Global Navigation Satellite Systems (GNSSs) is examined. A self-coherence anti-jamming scheme is introduced which relies on the unique structure of the coarse/acquisition (C/A) code of the satellite signals.					
<b>15. SUBJECT TERMS</b> Anti-jam GPS; Interference Suppression; Multipath Mitigation; Impulsive Noise; Antenna Array Processing; Self-Coherence					
<b>16. SECURITY CLASSIFICATION OF:</b>			<b>17. LIMITATION OF ABSTRACT</b> UU	<b>18. NUMBER OF PAGES</b>	<b>19a. NAME OF RESPONSIBLE PERSON</b> Dr. Moeness G. Amin
<b>a. REPORT</b> U	<b>b. ABSTRACT</b> U	<b>c. THIS PAGE</b> U			<b>19b. TELEPHONE NUMBER (Include area code)</b> 610-519-4599